SAND2011-5573C

Effects of Internal and External Hydrogen Environments on Crack Growth Susceptibility of an Iron Based Superalloy

N. R. Moody, W. M. Garrison, S. L. Robinson, and M. W. Perra

Sandia National Laboratories, Livermore, CA
Carnegie Mellon University, Pittsburgh, PA

Environmental Damage in Structural Materials
Engineering Conferences International
Krakow, Poland
August 14-19, 2011

Yield strength and microstructure control slow crack growth susceptibility in stainless steels and superalloys.

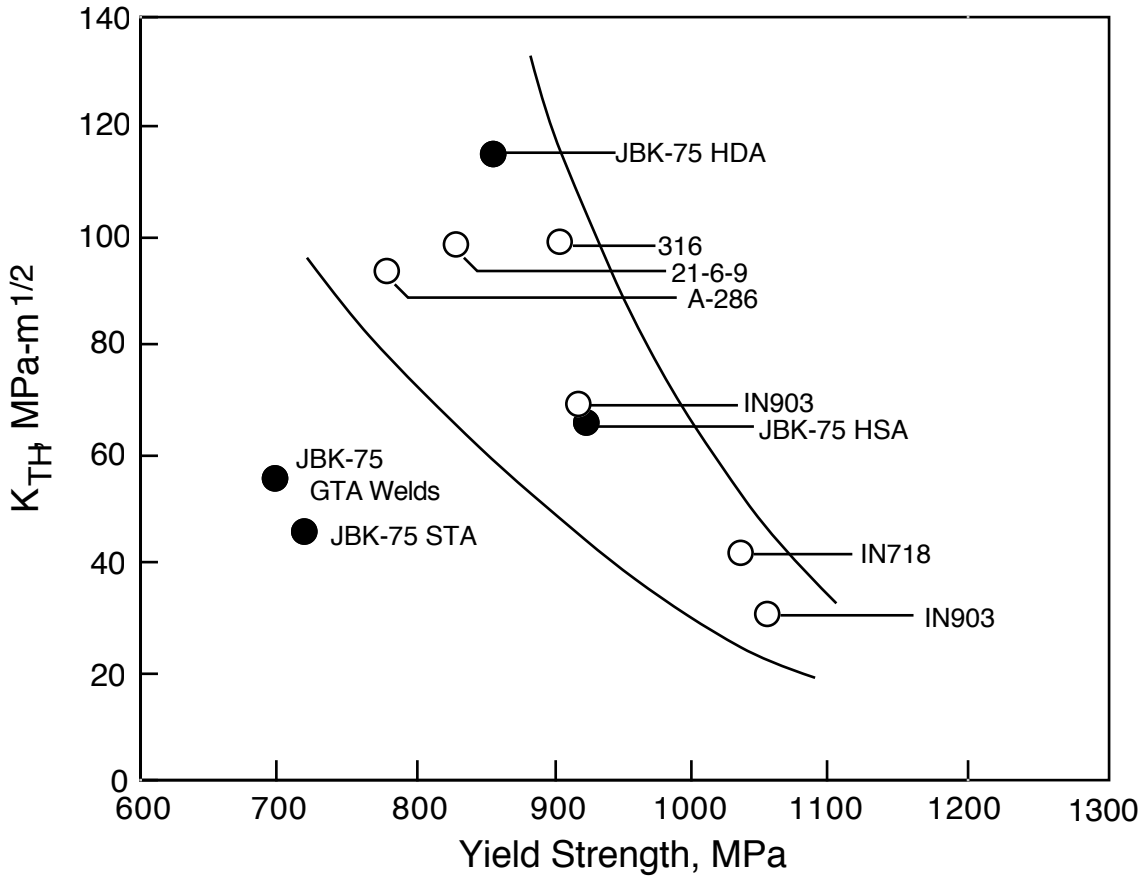

(Perra, 1977-1981)

Purpose

Define the role of environment on crack growth susceptibility in austenitic superalloys.

Approach

Combine results of previous studies and of unpublished work on the high strength iron based austenitic superalloy IN903.

Outline

Describe the microstructure and modes of deformation as they establish the modes of failure.

Discuss the effects of internal and external hydrogen on toughness, thresholds, and fracture processes.

Describe how hydrogen environment affects crack growth rates and fracture processes.

Show how microstructure interacts with hydrogen to establish crack growth behavior.

The microstructure of IN903 consists of equiaxed grains, annealing twins, grain boundary and large matrix carbides. This alloy is strengthened by 20-nm-diameter gamma’ precipitates

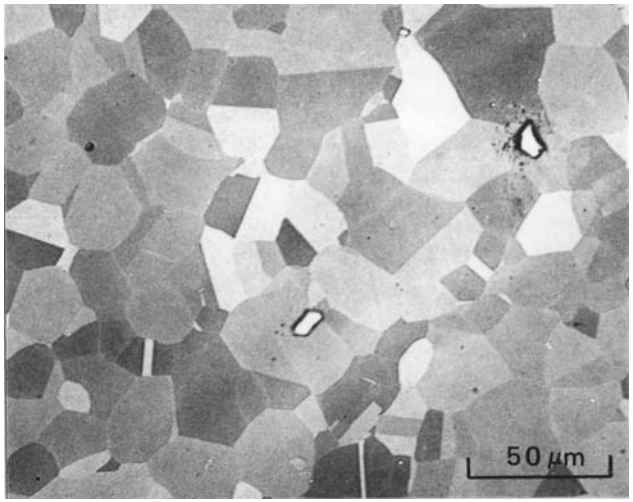

Optical Microstructure

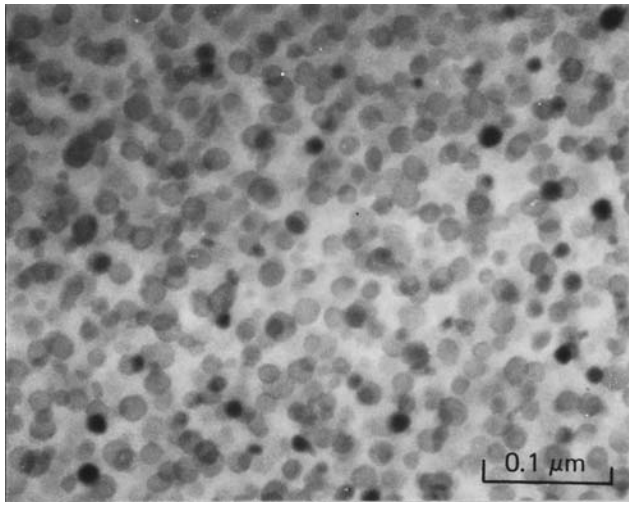

Gamma’ Precipitates

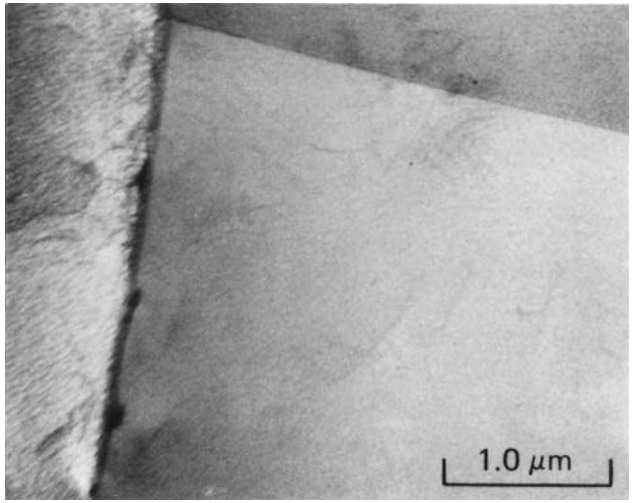

Grain Boundary Carbides

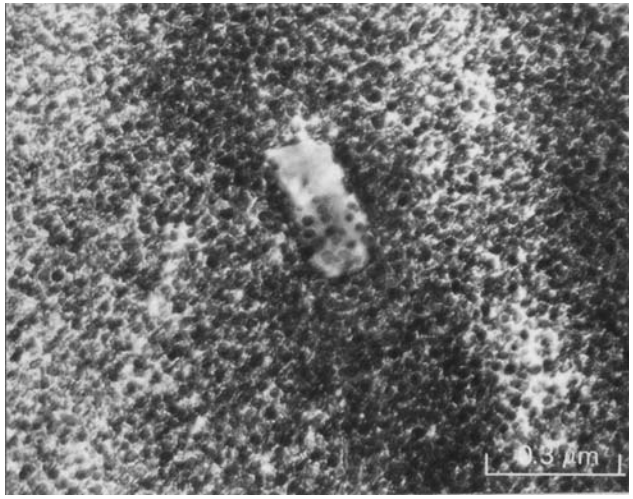

Matrix Carbides

Deformation in IN903 occurs by coplanar slip resulting in the dislocation cutting of gamma’ precipitates.

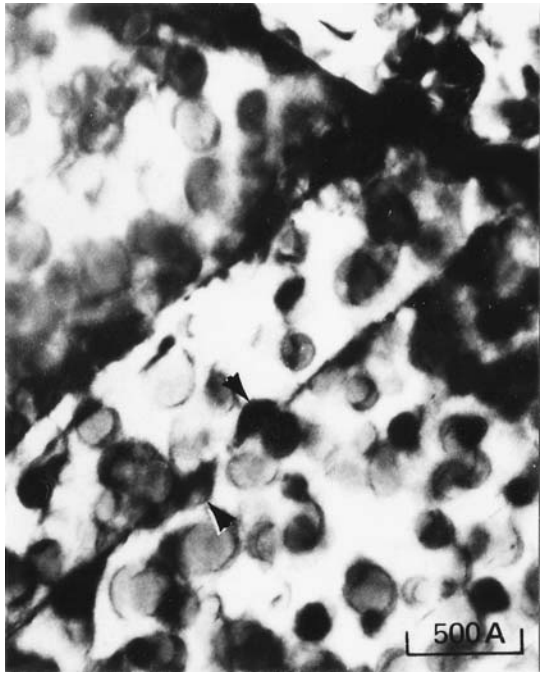

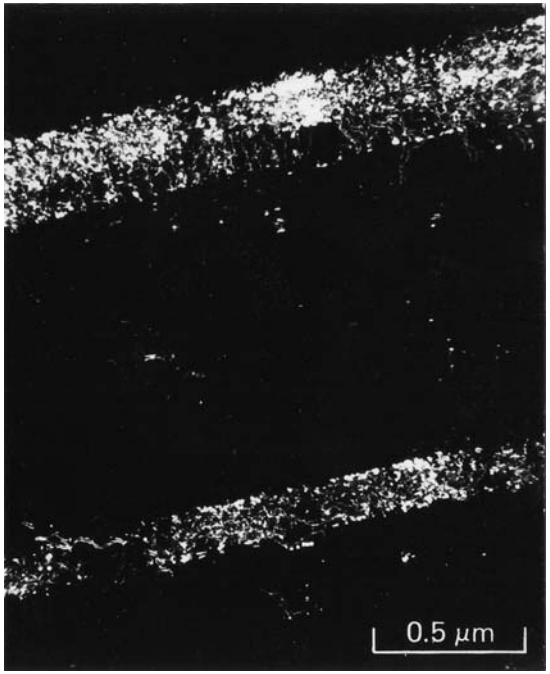

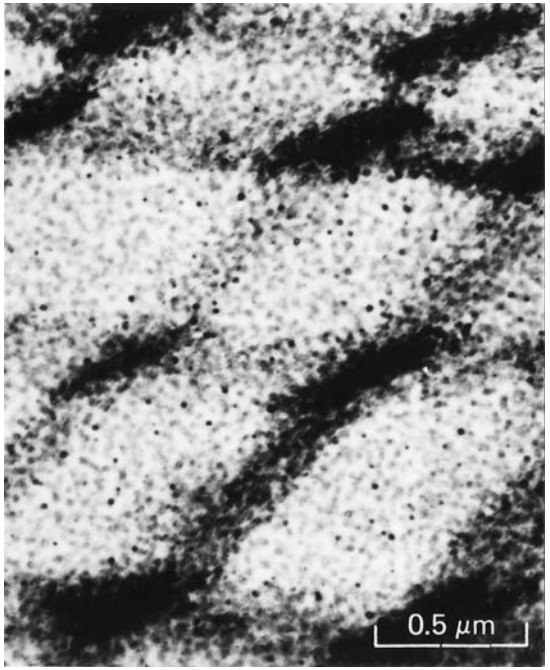

Hydrogen-induced crack growth often exhibits three stages of behavior with each stage defined by the mechanisms controlling fracture.

Susceptibility to crack growth depends on many factors.

- Internal
  - Composition
  - Microstructure
  - Strength
- External
  - Time
  - Stress
  - Stress state
  - Temperature
  - Environment

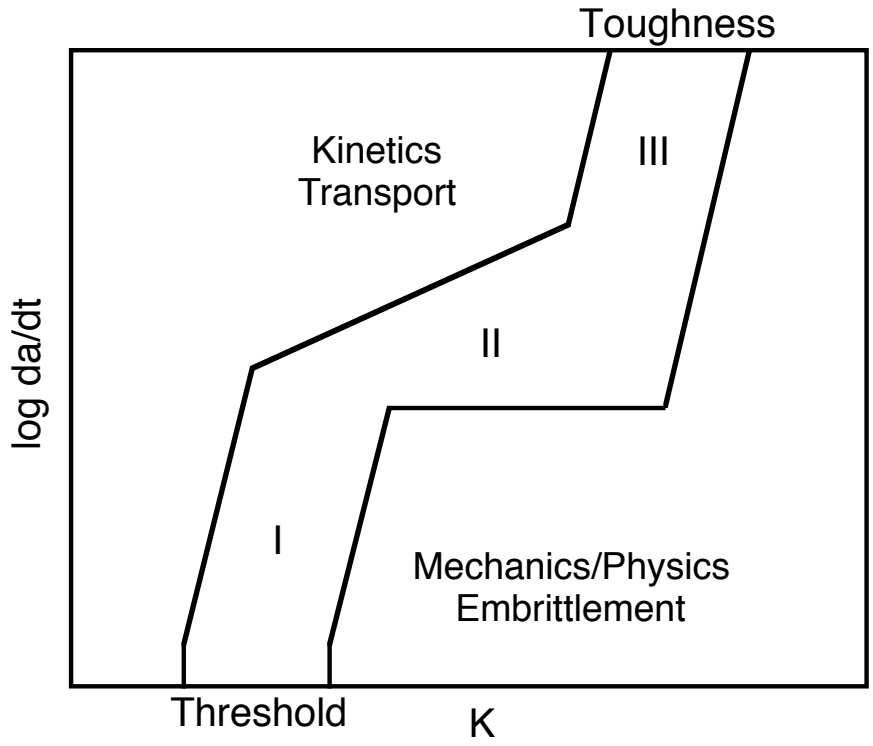

Increasing hydrogen concentration markedly reduced the fracture toughness of IN903.

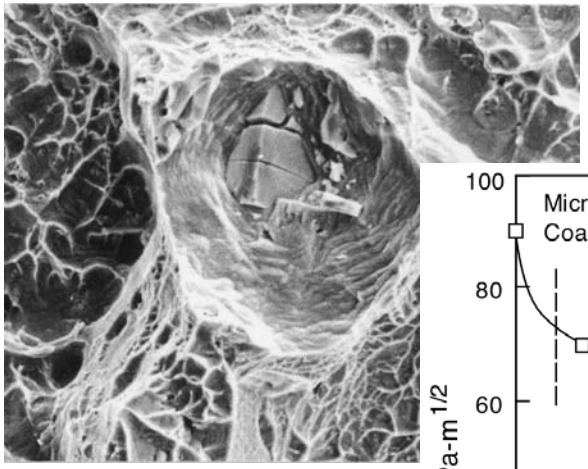

uncharged

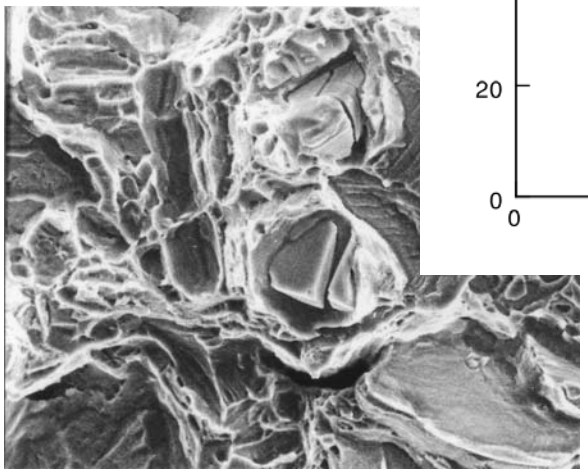

770 appm

Fracture Toughness
Charged Samples

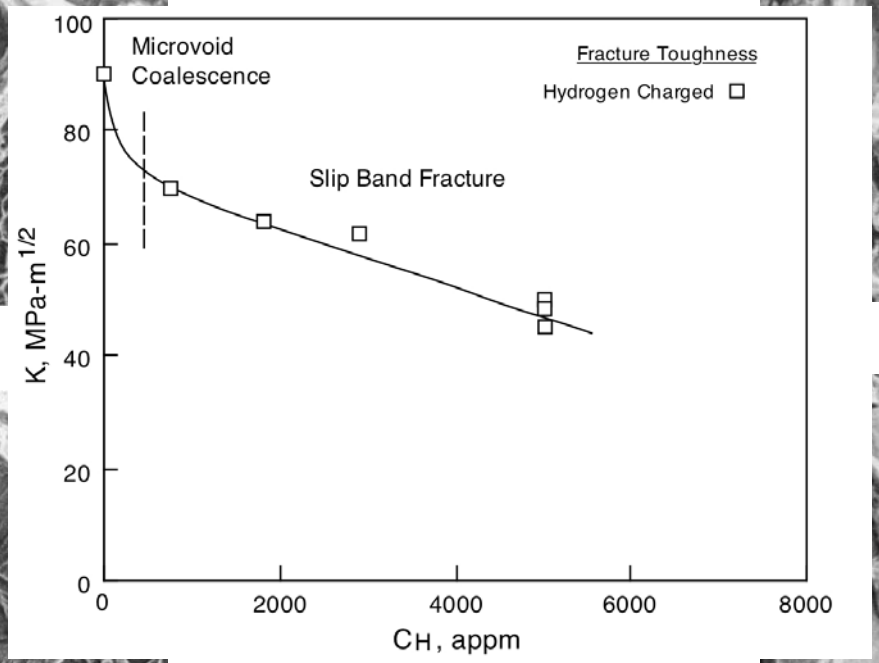

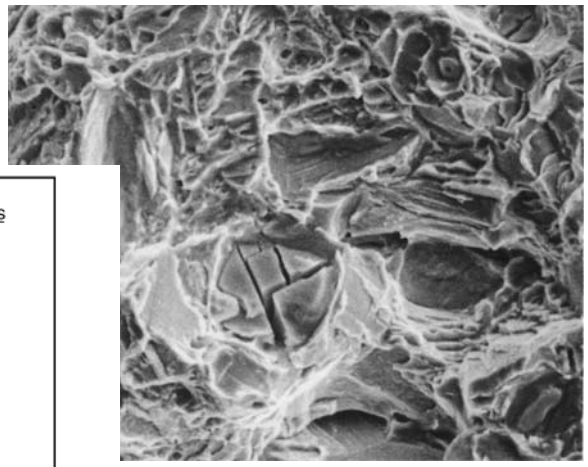

2900 appm

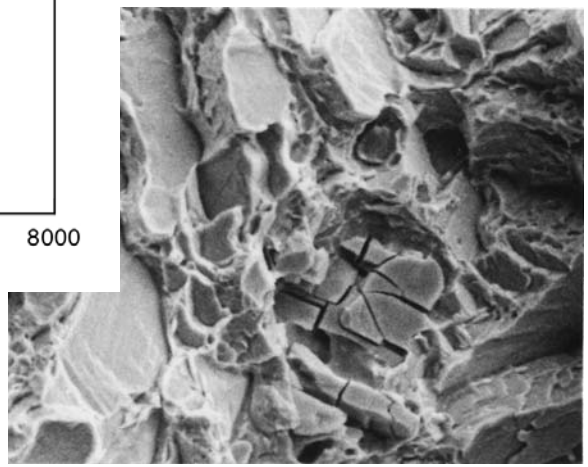

5000 appm

Slow crack growth thresholds in hydrogen charged samples are significantly lower than fracture toughness of hydrogen charged samples.

Slow Crack Growth-Charged Samples

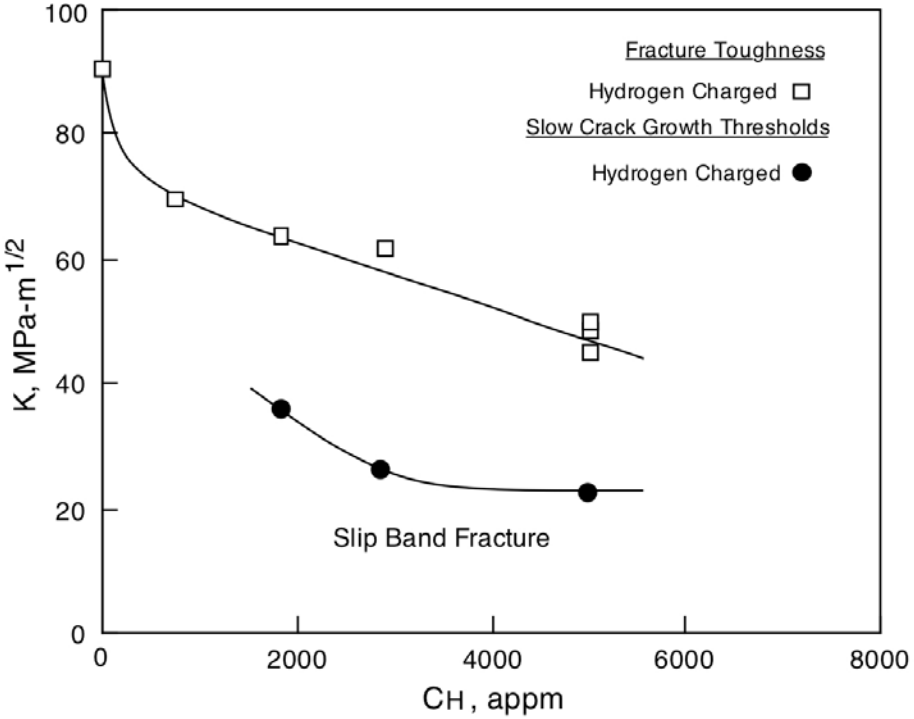

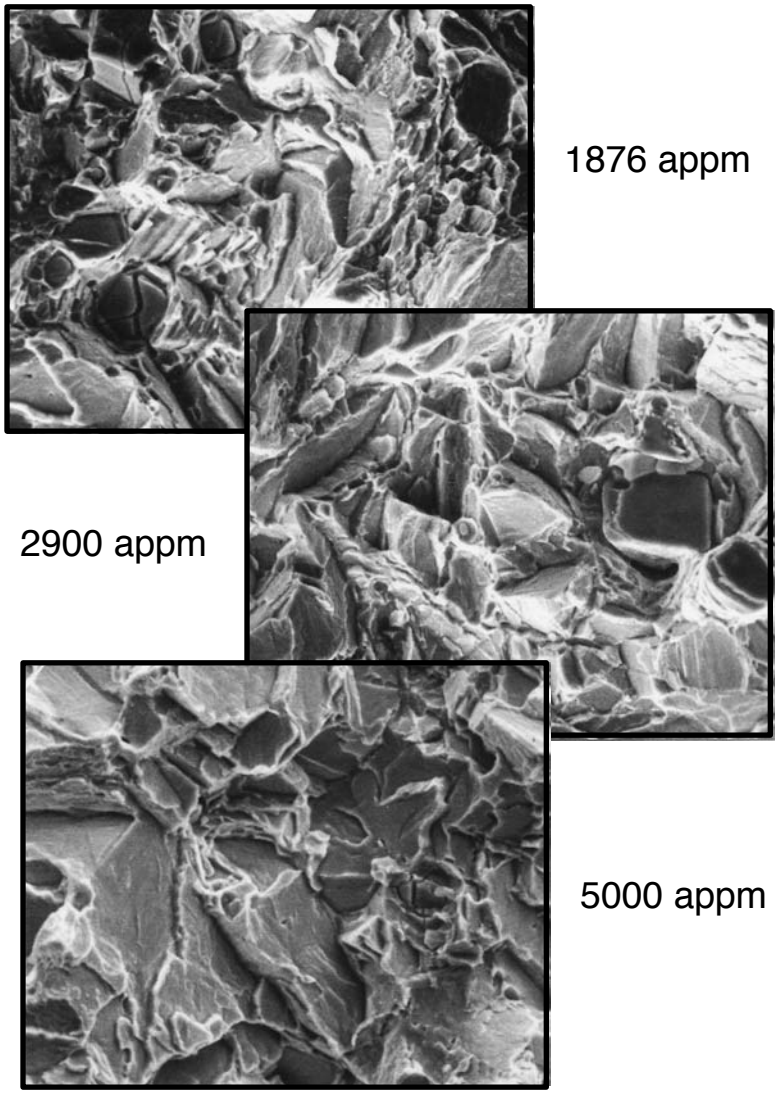

Slow crack growth thresholds for samples tested in hydrogen gas fall between the fracture toughness and slow crack growth thresholds in hydrogen charged samples.

Slow Crack Growth-Hydrogen Gas

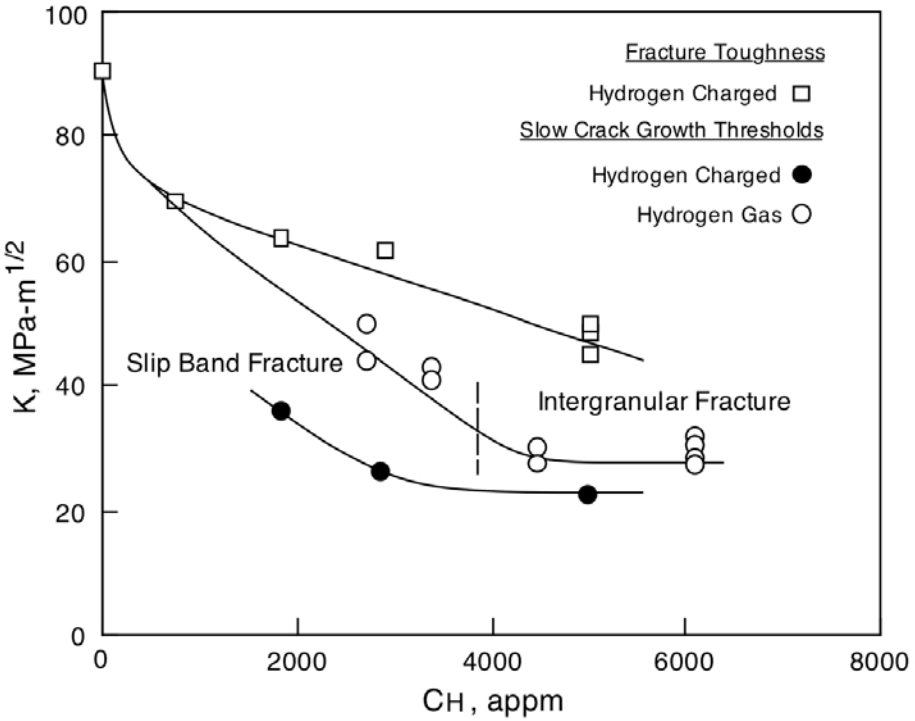

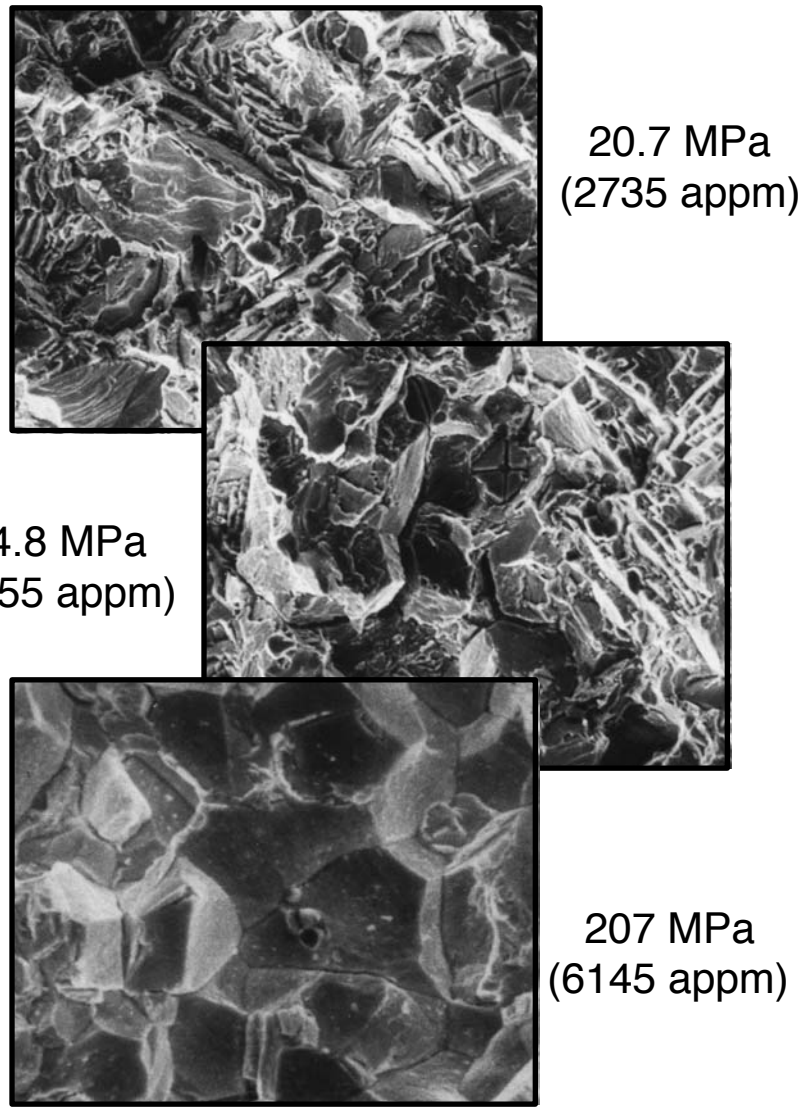

20.7 MPa
(2735 appm)

44.8 MPa
(3355 appm)

207 MPa
(6145 appm)

Fracture modes exhibit a nominal progression from microvoid coalescence to slip band failure and finally intergranular failure with increasing hydrogen concentration.

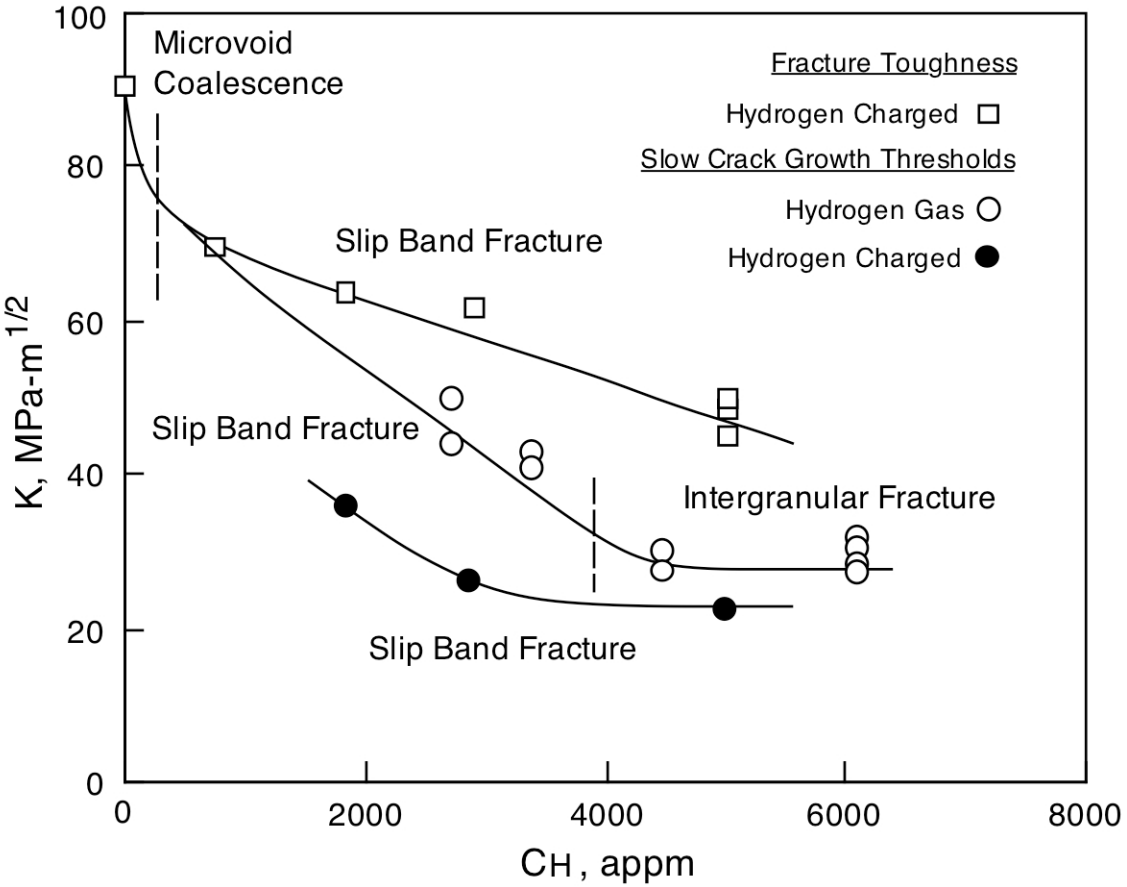

Comparing void growth at failure indicates that crack tip hydrogen concentrations increase during slow crack growth.

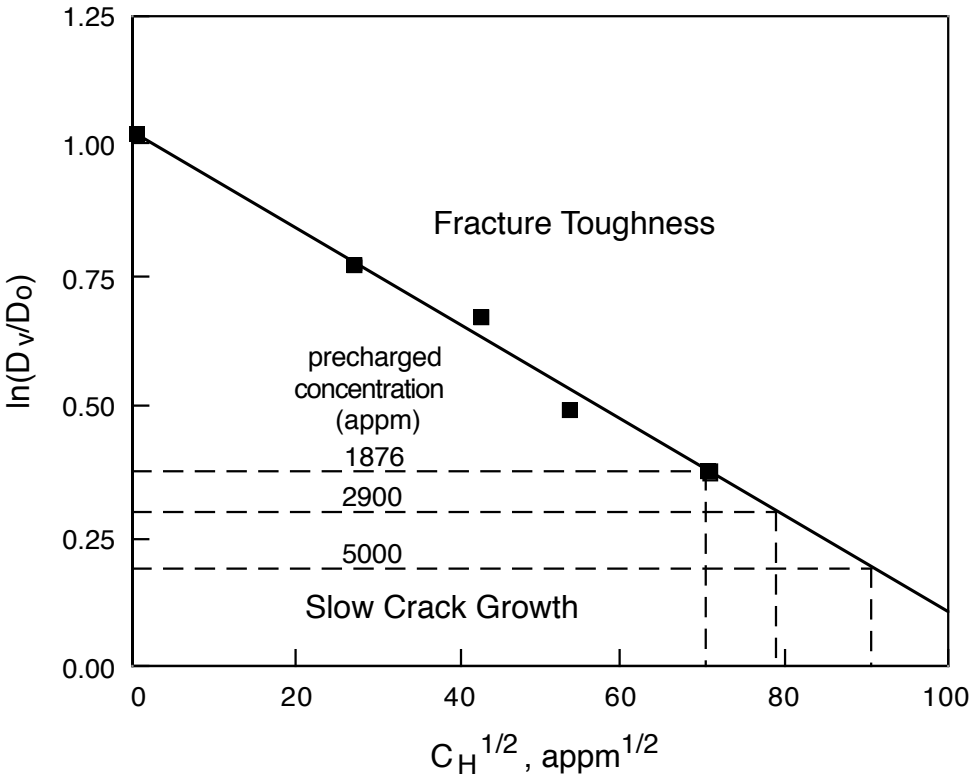

Fracture Toughness

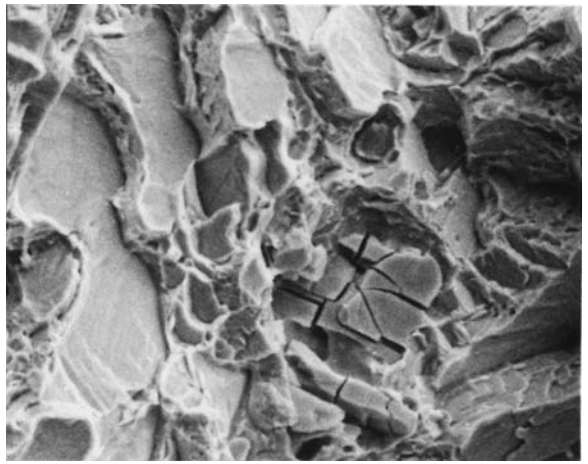

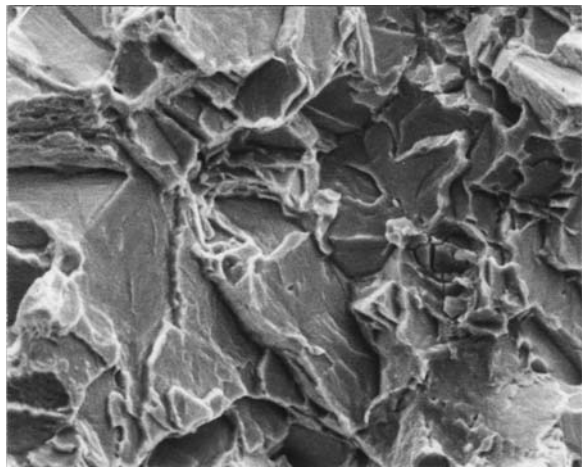

Slow Crack Growth

A strong interaction between hydrogen and the crack tip stress field alters diffusion paths and enhances hydrogen concentration.

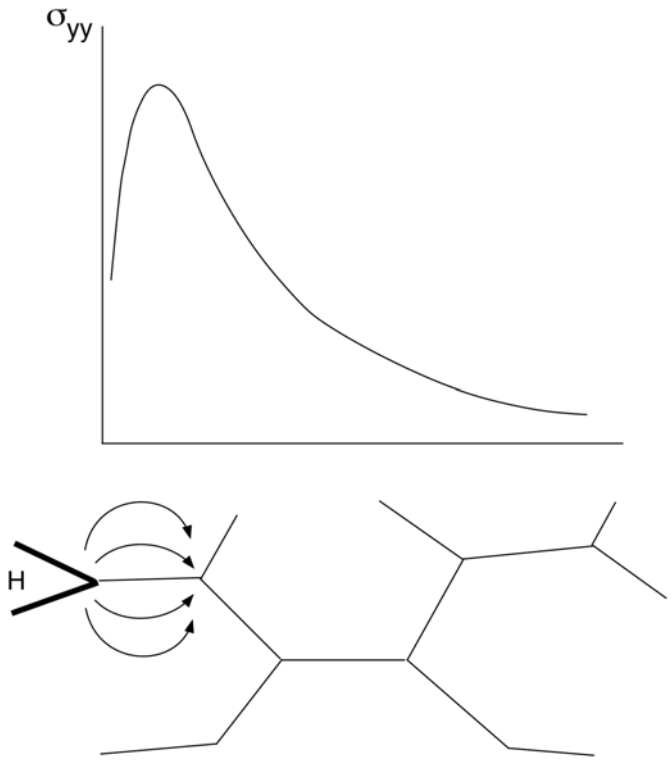

The effect is through lattice concentration.

$$C_{total}(\sigma) = C_{lattice}(\sigma) + C_{trap}(\sigma)$$

where

$$C_{lattice}(\sigma) = C_{lattice}(0)\exp(\sigma_h V_H / RT)$$

Crack tip stresses significantly enhance hydrogen concentrations in the near crack tip regions.

	P(0) atm	f(0) atm	CL(0) appm	CT(0) appm	Ctot(0) appm	CL(σ) appm	CT(σ) appm	Ctot(σ) appm
KQH	68	74	26	748	774			
	340	443	165	1711	1876			
	680	1159	411	2489	2900			
	1360	3057	1290	3710	5000			
KIH	340	443	165	1711	1876	2381	4315	6696
	680	1159	411	2489	2900	2864	4414	7279
	1360	3057	1290	3710	5000	4015	4568	8583
KTH	204	251	363	2371	2734	1695	4096	5791
	408	593	559	2796	3355	2534	4353	6887
	1020	2044	1037	3469	4506	3503	4508	8011
	2040	7465	1982	4154	6136	5794	4692	10485

Thresholds in charged samples are lower than toughness and threshold values in hydrogen gas even when crack tip stress effects are included in the hydrogen concentration calculations.

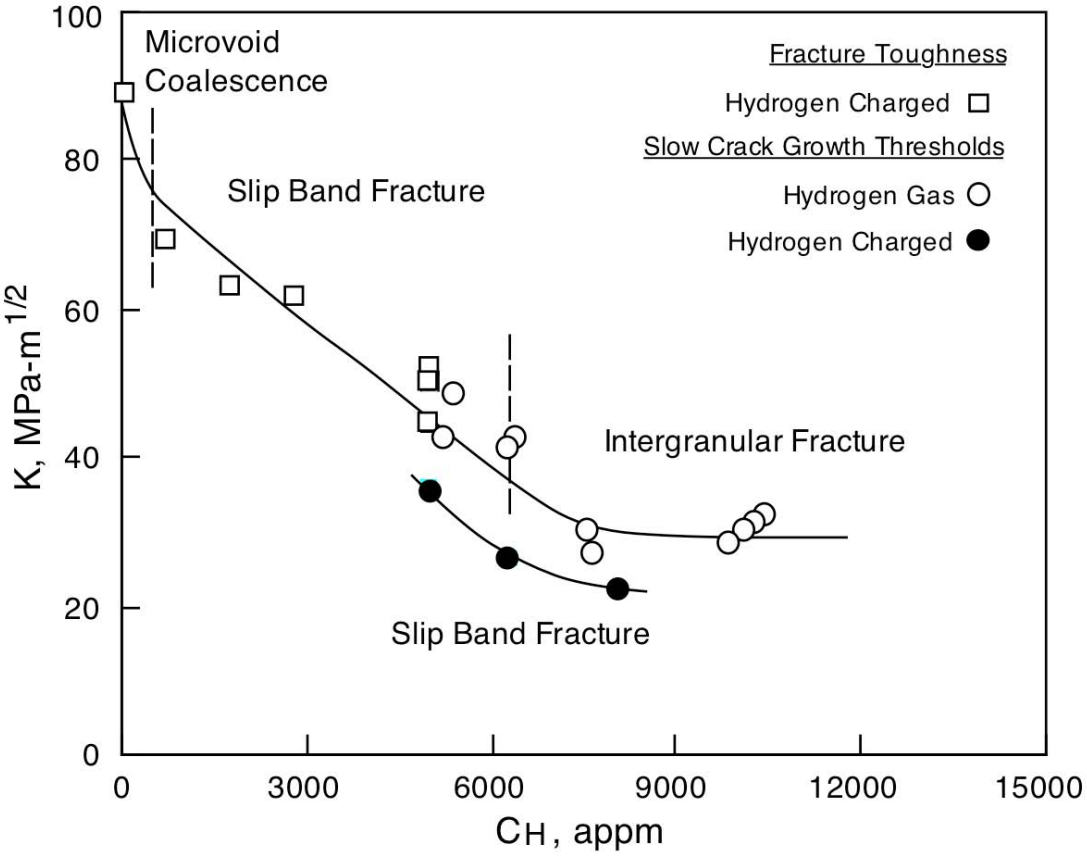

Results show that additional factors affect crack growth.

Transition from critical strain to critical stress control as hydrogen pressure (concentration) increases

Critical Strain

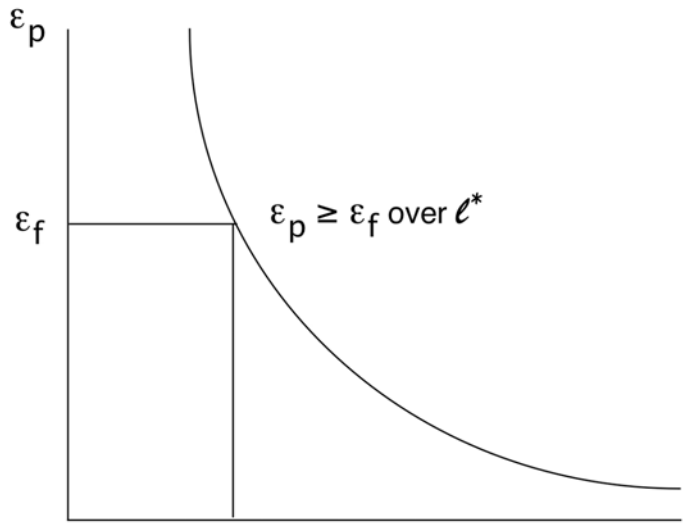

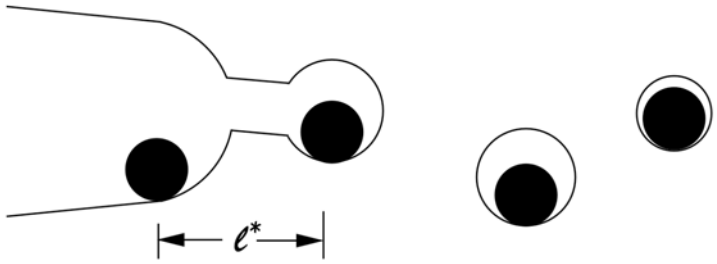

Slip Band Fracture

Critical Stress

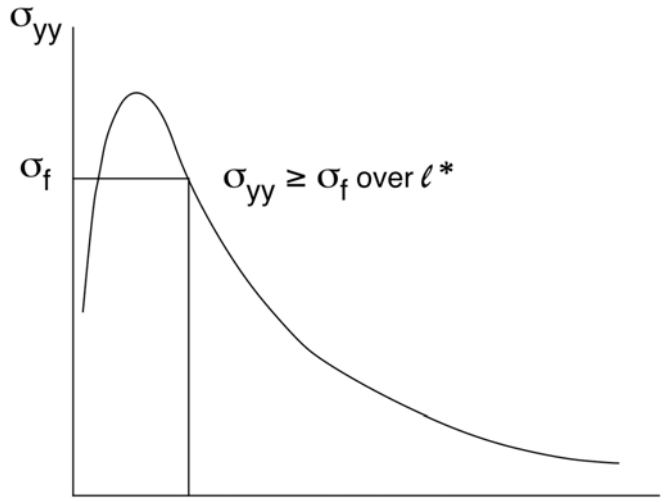

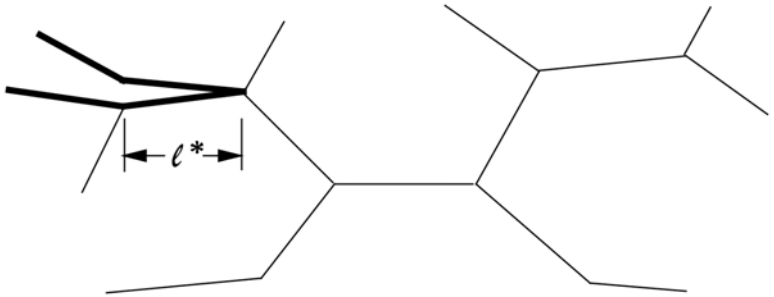

Intergranular Fracture

A ratio of √2 exists between slow crack growth thresholds and the stage I/II transitions in IN903 and bcc steels, charged with hydrogen and tested in hydrogen gas.

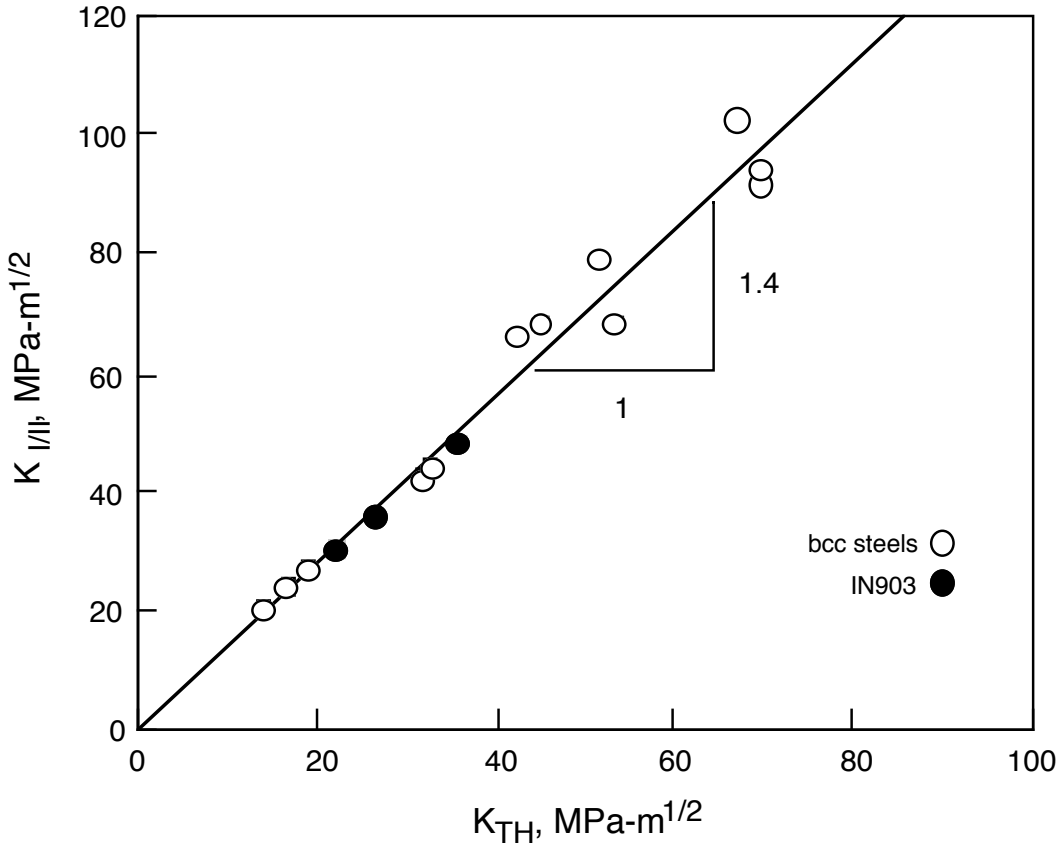

This behavior observed with slip band, quasi-cleavage and intergranular fracture modes.

For IN903, slip band fracture is a strain controlled process with fracture toughness governed by average matrix carbide spacing and slow crack growth thresholds by nearest neighbor carbide spacing.

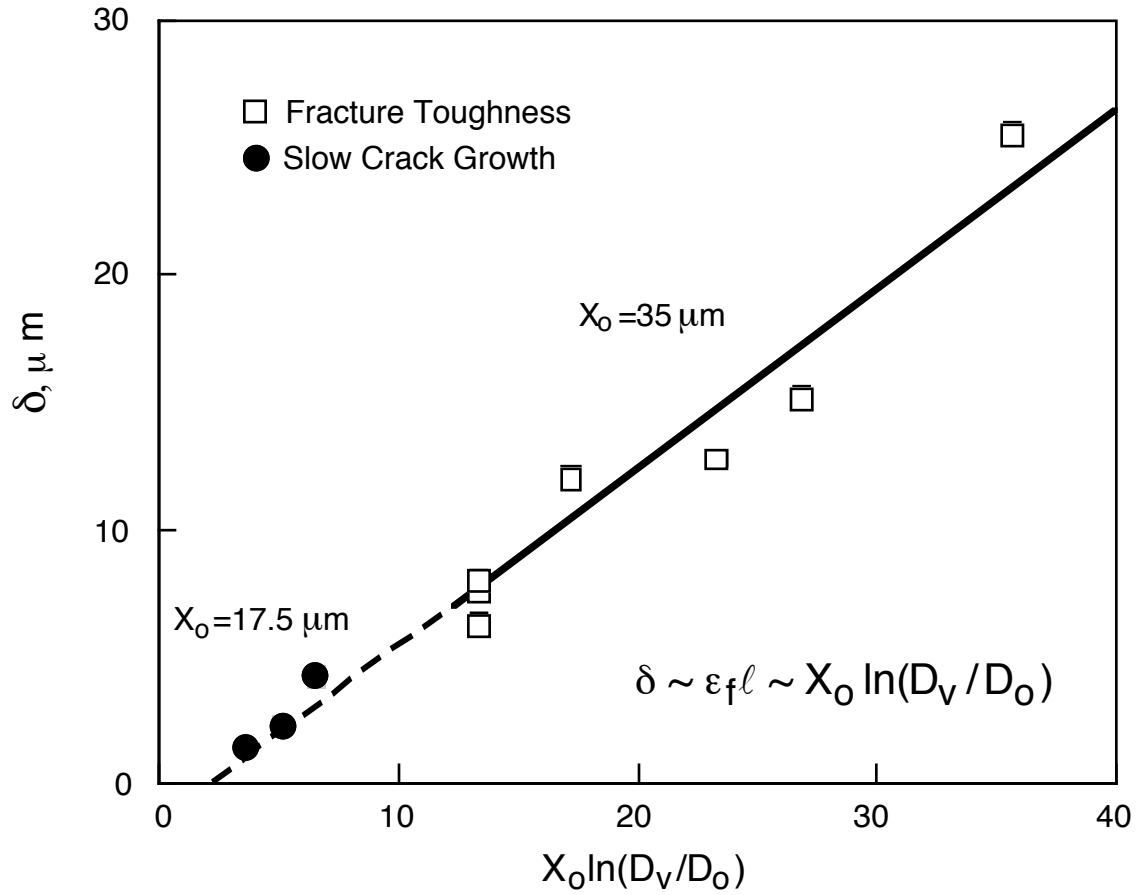

Fracture changes from lateral growth along the main crack front to forward growth as the characteristic fracture distance changes from nearest neighbor to average carbide spacing.

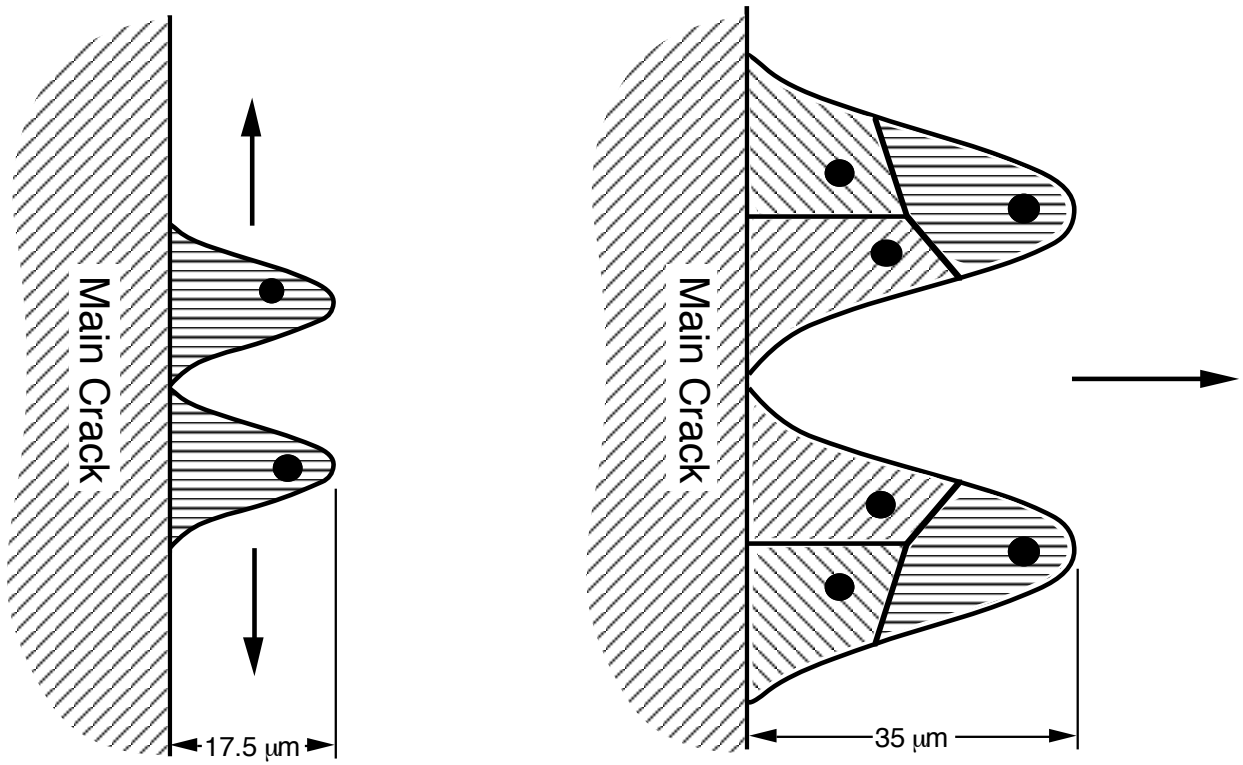

Threshold / Stage I

Stage I/II Transition

This behavior occurs with slip band, quasi-cleavage and intergranular fracture modes.

Thresholds and toughness vary monotonically with hydrogen concentration when normalized to the controlling fracture distances and crack tip stress effects are included in the concentration calculations.

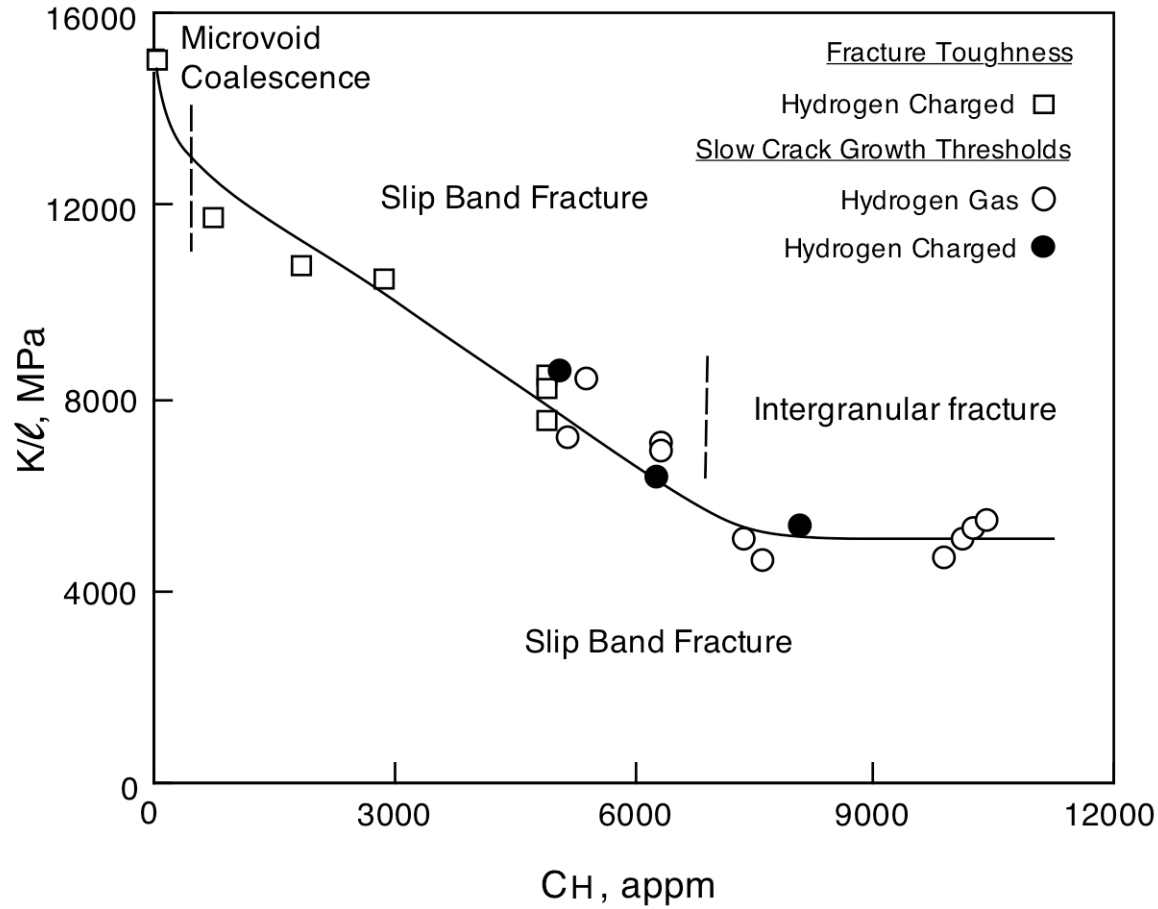

The superposition of slip band and intergranular fracture modes indicates there are differences due to hydrogen environment.

Crack growth rates and fracture processes vary markedly with pressure (concentration) in a hydrogen gas environment.

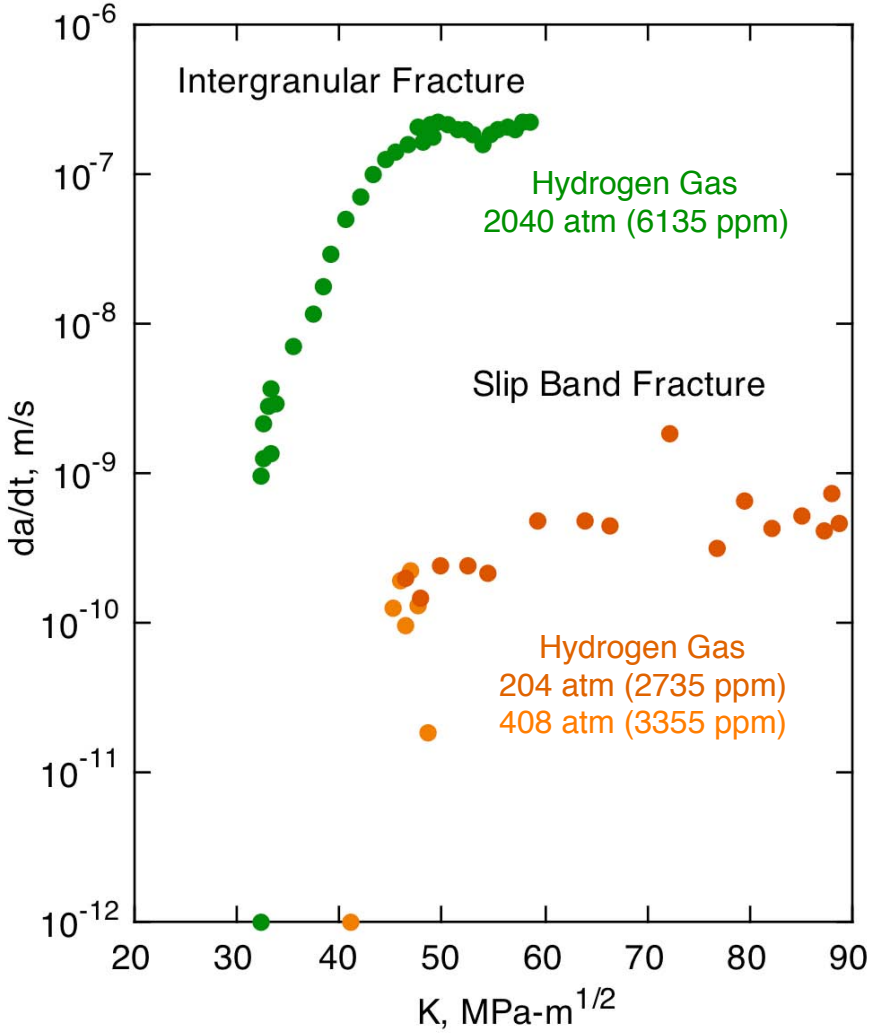

Intergranular Fracture

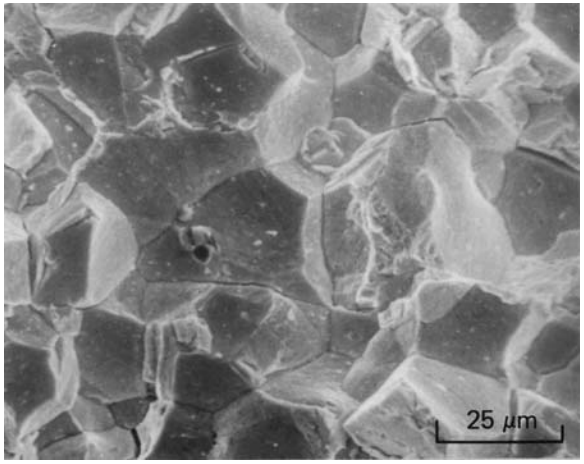

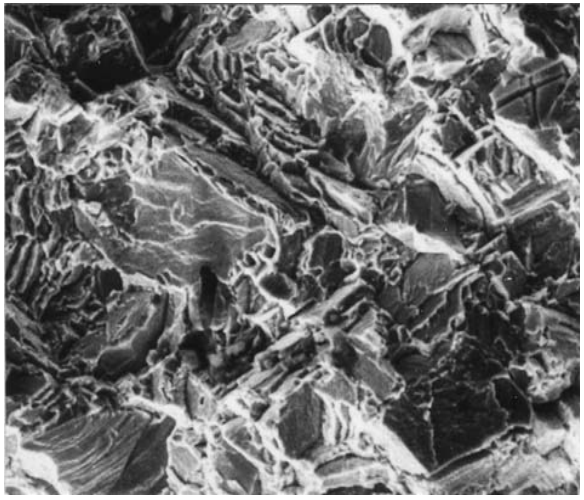

Slip Band Fracture

Crack growth rates exhibit markedly different behaviors with respect to hydrogen concentration and hydrogen environment.

Intergranular Fracture

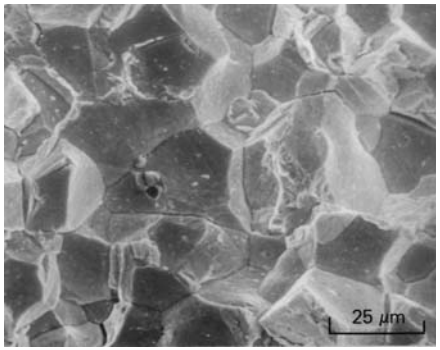

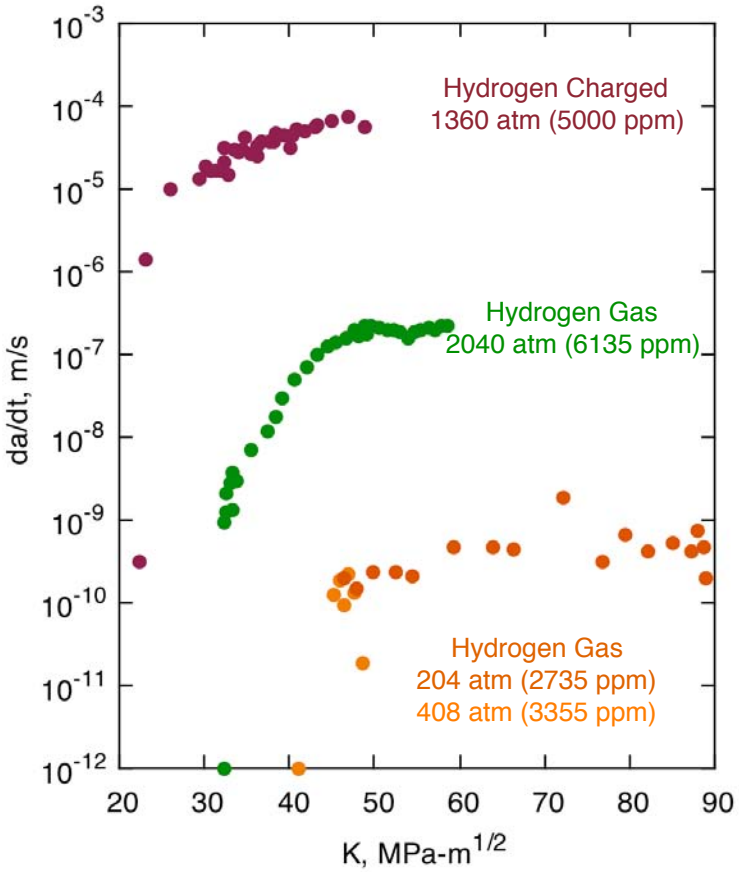

Slip Band Fracture

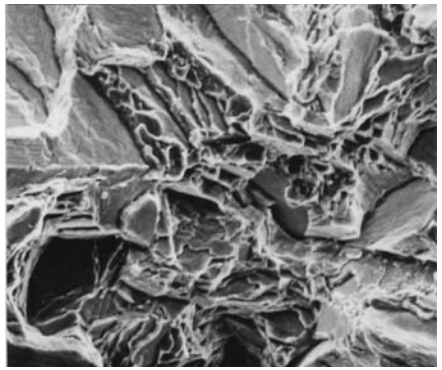

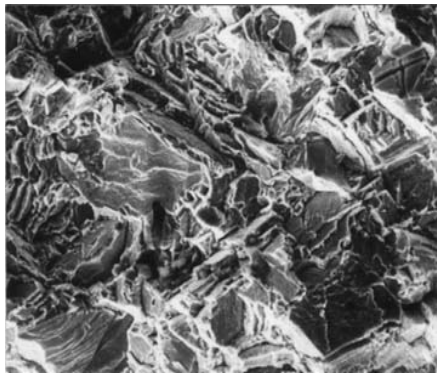

Slip Band Fracture

Unlike toughness and thresholds, crack growth rates and fracture modes do not vary in a predictable manner.

Fracture initiates at matrix carbides and proceeds along coplanar slip bands.

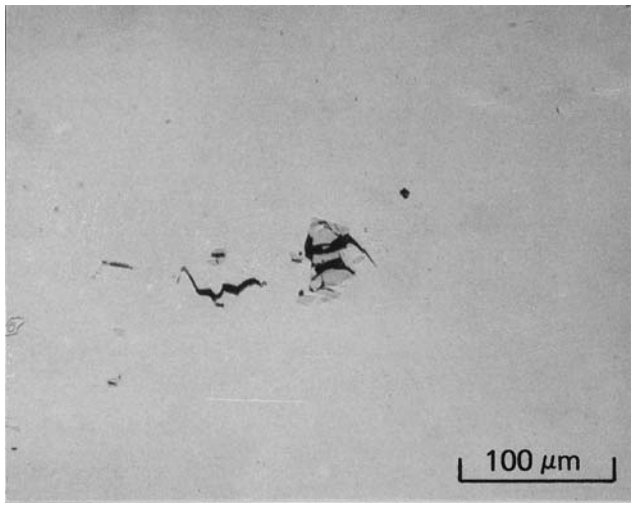

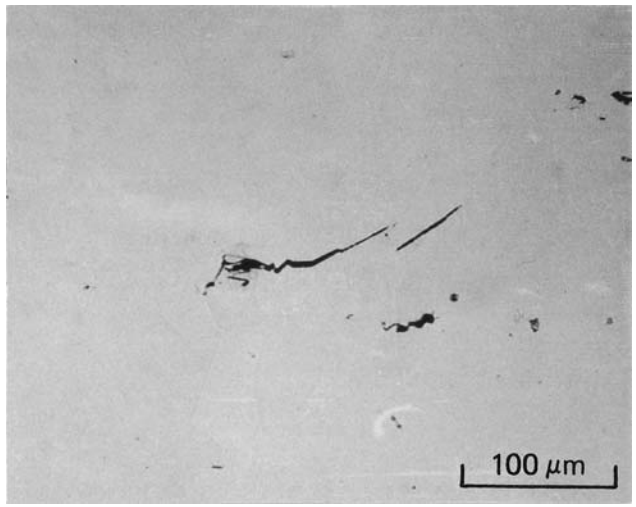

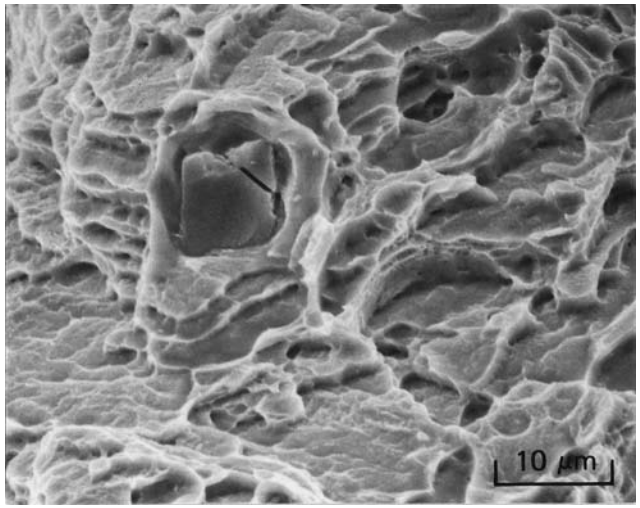

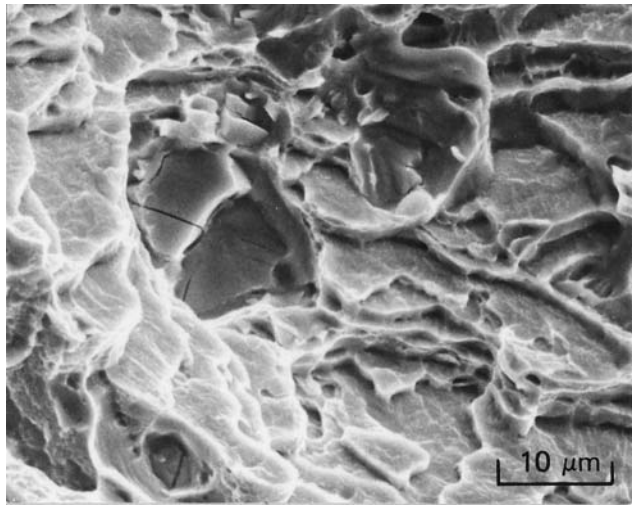

Intersecting slip bands create offsets which block dislocation motion. The high dislocation density within these intersections and destruction of order promotes void formation.

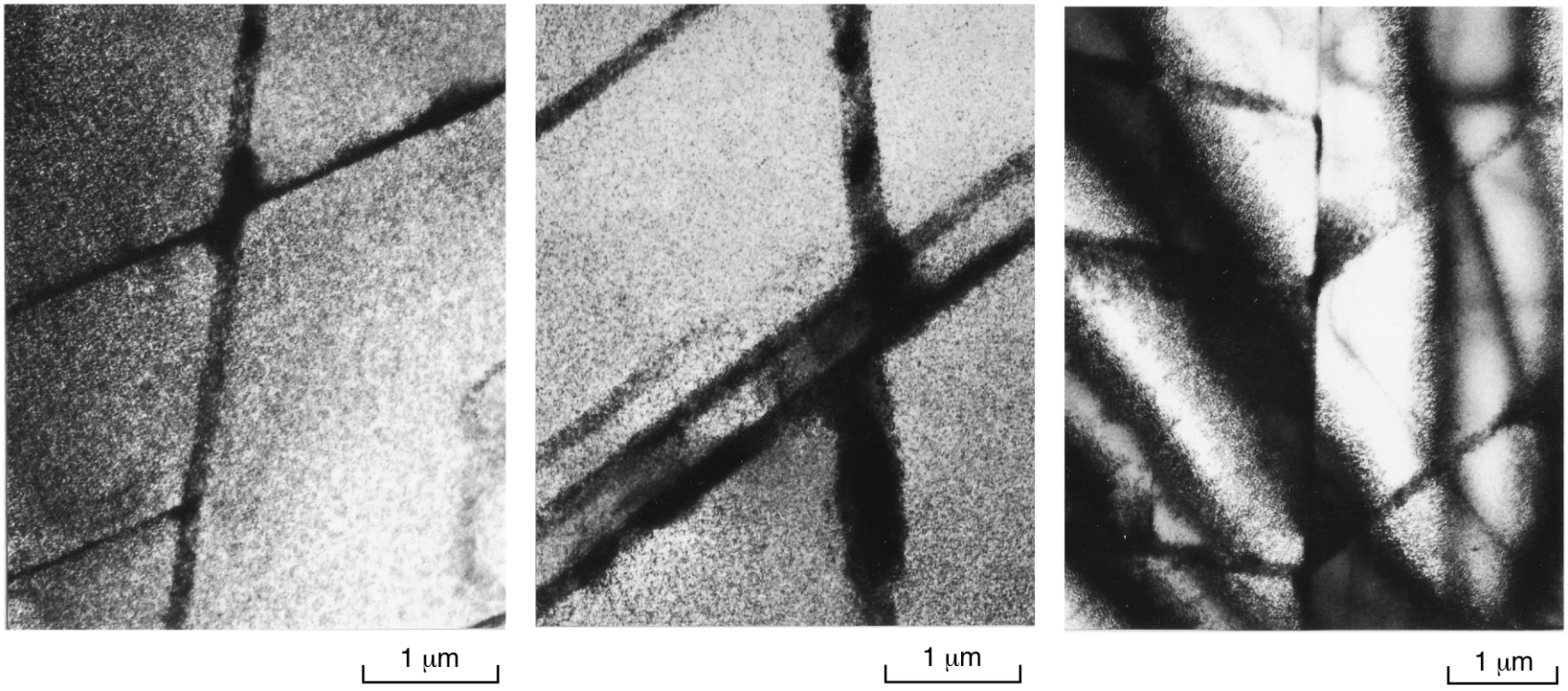

Trap site energies show that significant trapping of hydrogen can occur at an a/2[110] Lomer-Cottrell Lock.

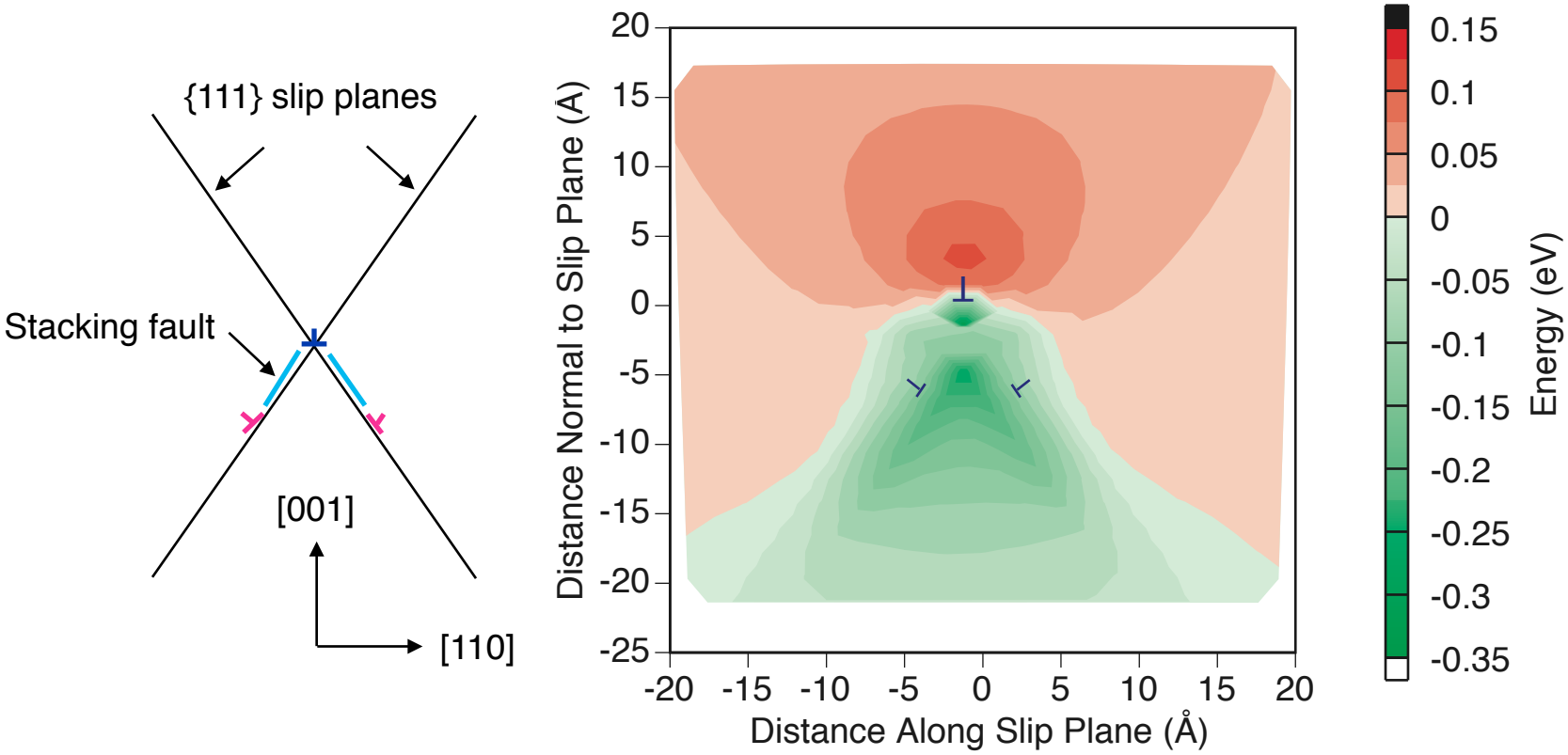

The a/2 [110] Lomer dislocation has a maximum trap energy of 0.32 eV at the core of the a/6[110] stair rod

Void formation at intersecting slip bands is followed by failure of inter-connecting slip band segments.

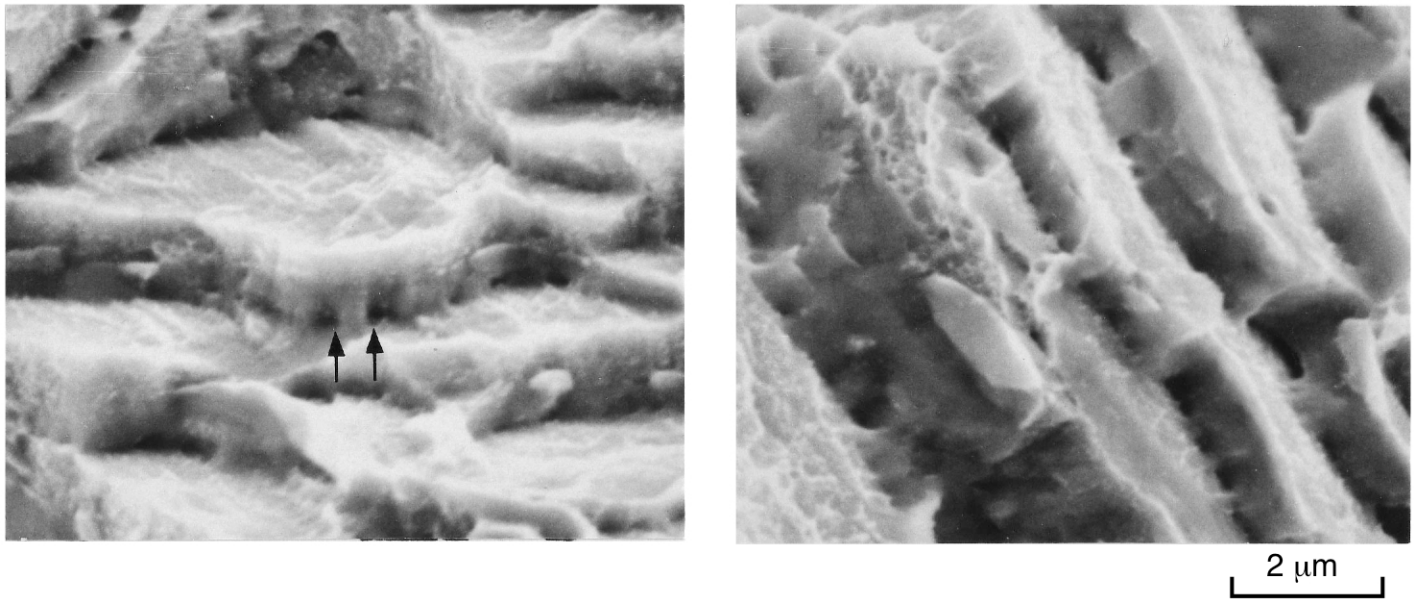

The intersecting slip bands create high energy trap sites (0.3 eV) where hydrogen segregates leading to void formation.

Hydrogen-induced stage II crack growth occurs by a sequence of two distinct fracture processes.

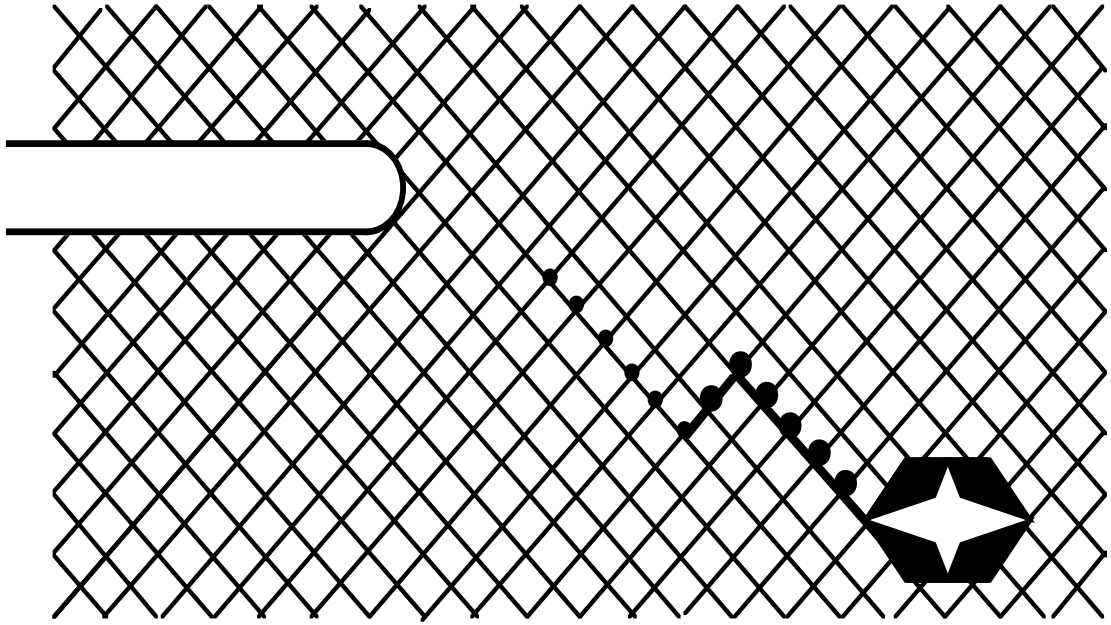

Crack growth begins with fracture of matrix carbides ahead of the main crack forming microcracks.

The microcracks then trigger void formation at slip band intersections and failure of inter-connecting slip band segments.

We have developed a model based on Fick's Second Law for diffusion, trapping at dislocation intersections, and a critical strain criterion for fracture.

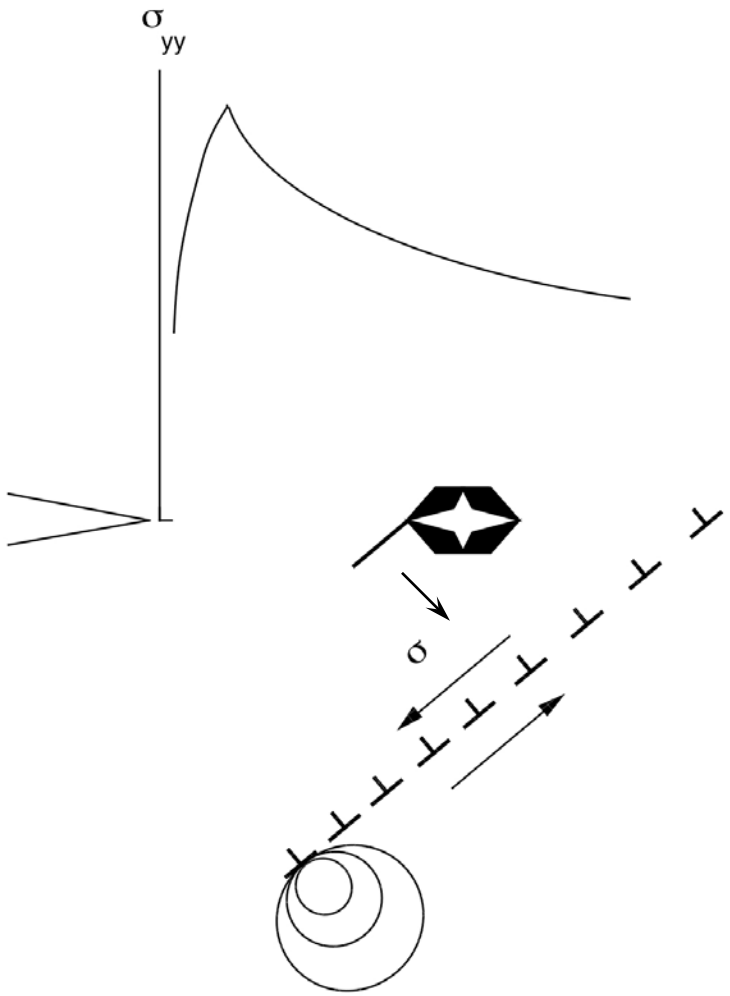

Fracture of matrix carbides:

Diffusion and Accumulation:

$$\frac{1}{D}\frac{\partial c}{\partial t} = \Delta c + \frac{\nabla(c\nabla V)}{kT}$$

Stress Field Interactions:

$$V = -\frac{8\pi(1+\nu)\sqrt{|}}{3}\varepsilon r_i^3 \sigma \frac{\sin(\theta/2)}{\sqrt{r}}$$

Trapping:

$$\frac{C}{1\text{-}C} = C_o \exp\left(\frac{E_b}{RT}\right)$$

Fracture:

$$\varepsilon_f^* = \varepsilon_{f_o}^* - \alpha C_H^{1/4}$$

The maximum normal stress ahead of the main crack front causes the matrix carbides to fracture. These fractured carbides then act as microcracks.

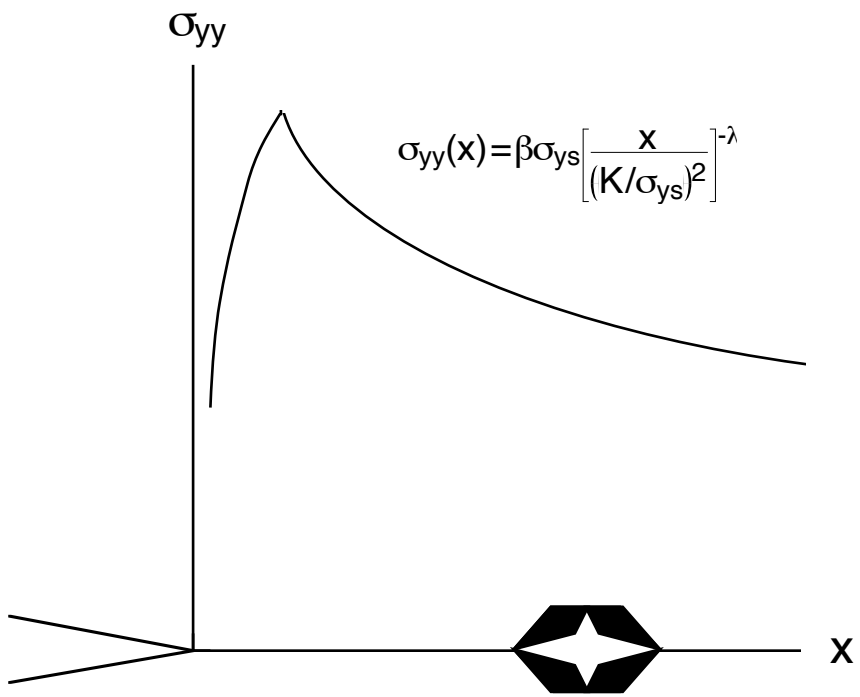

The conditions along theta=0 are a good approximation for all theta of interest.

$$k_f=\beta'\sqrt{\pi a}\left[1+\sum_{n=1}^{\infty}\left(\alpha_2+\frac{x_c}{a}\alpha_{2n-1}\right)x\frac{(2n)!}{(n!)^2}\left(\frac{a}{2x_c}\right)^{2n}\right]$$

$$k_h=\beta'\sqrt{\pi a}\left[1+\sum_{n=1}^{\infty}\left(\alpha_{2n}-\frac{x_c}{a}\alpha_{2n-1}\right)x\frac{(2n)!}{(n!)^2}\left(\frac{a}{2x_c}\right)^{2n}\right]$$

where

$$\beta'=\beta\sigma_{ys}\left[x_c/(K/\sigma_{ys})^2\right]^{-\lambda}$$

$$\alpha_n=\frac{(-1)^n\lambda(\lambda+1)\cdots(\lambda+n+1)}{n!}$$

Kameda

Lyubov and Vlasov modeled the interaction between hydrogen and stresses at the head of a slip band using a blocked array of edge dislocations.

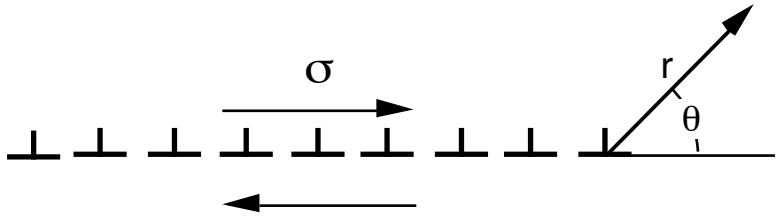

Lyubov and Vlasov

The interaction energy between an impurity atom and a dislocation pile-up is described by:

$$V=-\frac{8\pi(1+\nu)\sqrt{l}}{3}\varepsilon r_i^3\sigma\frac{\sin(\theta/2)}{\sqrt{r}}$$

The resulting redistribution of impurity atoms is then obtained from Fick's Second Law:

$$\frac{1}{D}\frac{\partial c}{\partial t}=\Delta c+\frac{\nabla(c\nabla V)}{kT}=Dc-L_1\sqrt{-}\left(\frac{\sin(\theta/2)}{r\sqrt{r}}\frac{\partial c}{\partial r}+\frac{\cos(\theta/2)}{r^2\sqrt{r}}\frac{\partial c}{\partial\theta}\right)$$

To a first approximation with terms for trapping, this reduces to:

$$\frac{C}{1-C}=C_o\left[1-\frac{A}{kT}\sqrt{\frac{l}{r}}\sin\frac{\theta}{2}\left\{\operatorname{erfc}\left(\frac{\rho-1}{2\sqrt{\tau}}\right)-\exp\left(\frac{\rho-1}{2}+\frac{\tau}{4}\right)\operatorname{erfc}\left(\frac{\rho-1}{2\sqrt{\tau}}+\frac{\sqrt{\tau}}{2}\right)\right\}\right]\exp\left(\frac{E_b}{RT}\right)$$

The effect of hydrogen on the critical strain for fracture along slip band segments can be determined from fracture toughness values and finite strain distributions.

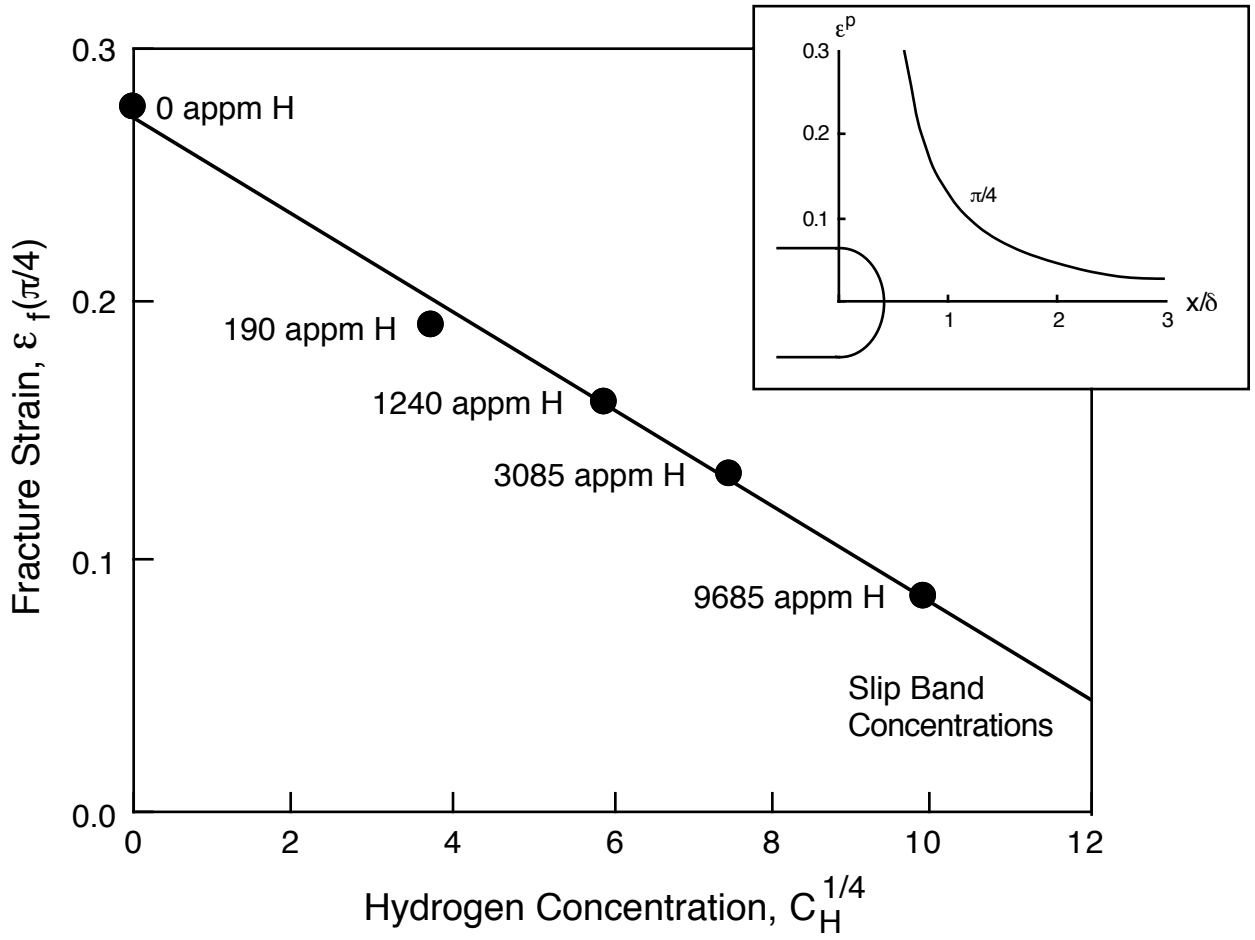

Predicted stage IIa crack growth rates are in reasonably good agreement with measured values at room temperature.

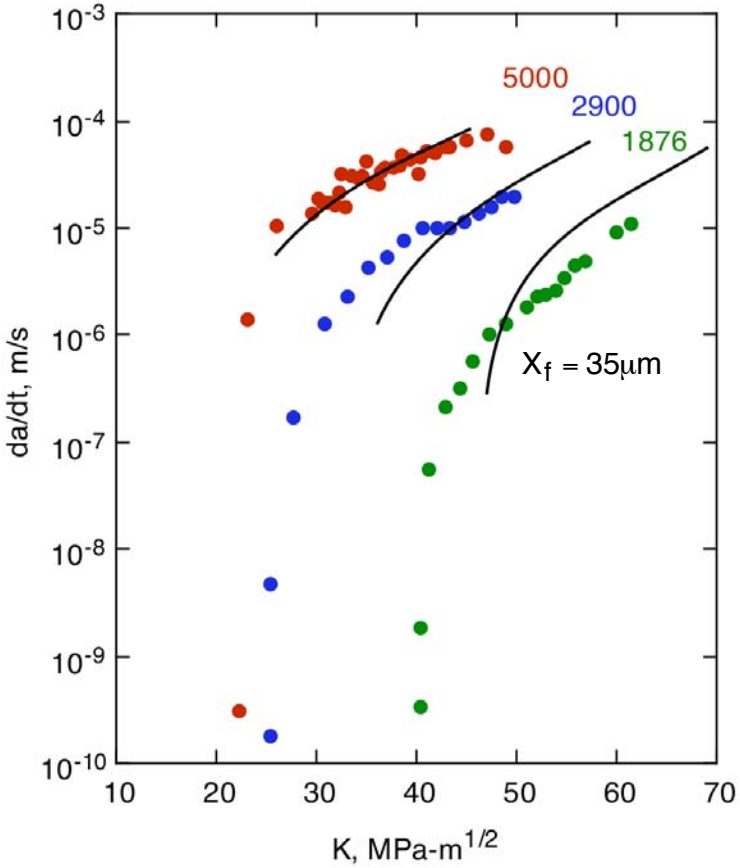

Concentration

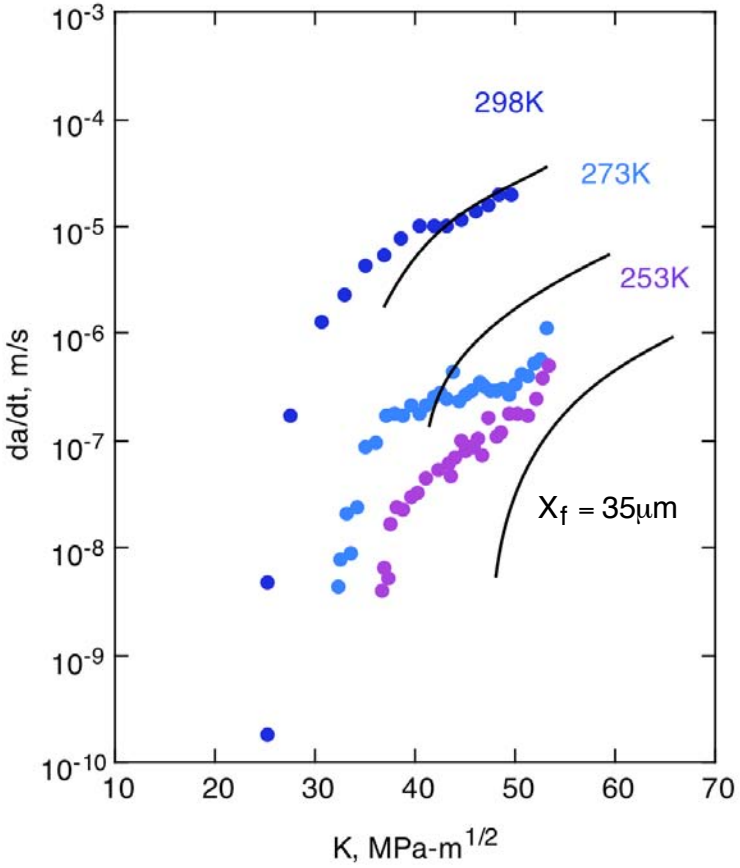

Temperature

Predicted stage IIa crack growth rates are in reasonably good agreement with measured values at room temperature.

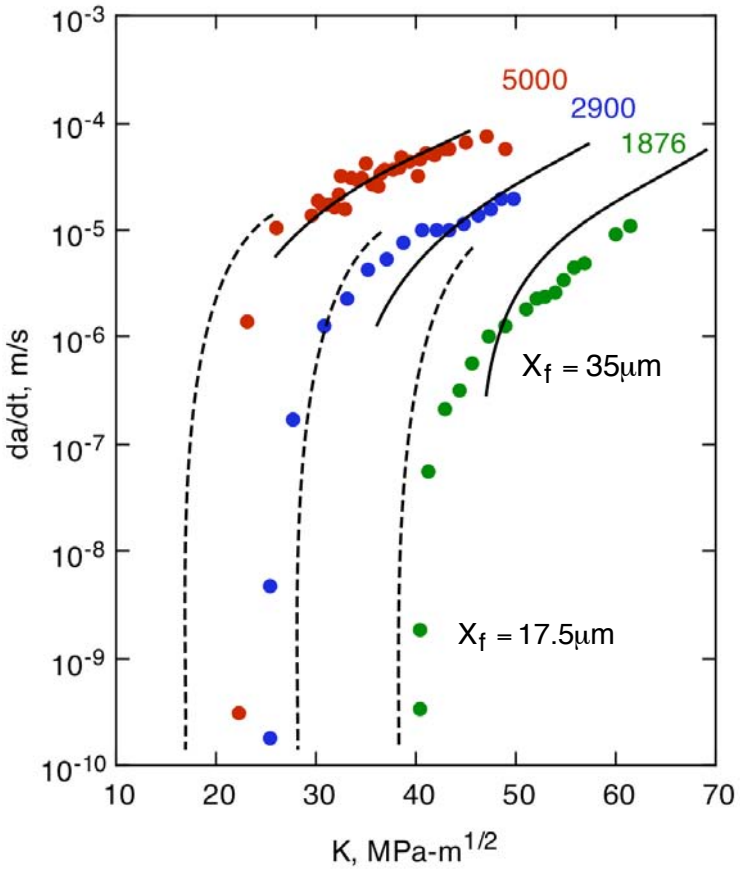

Concentration

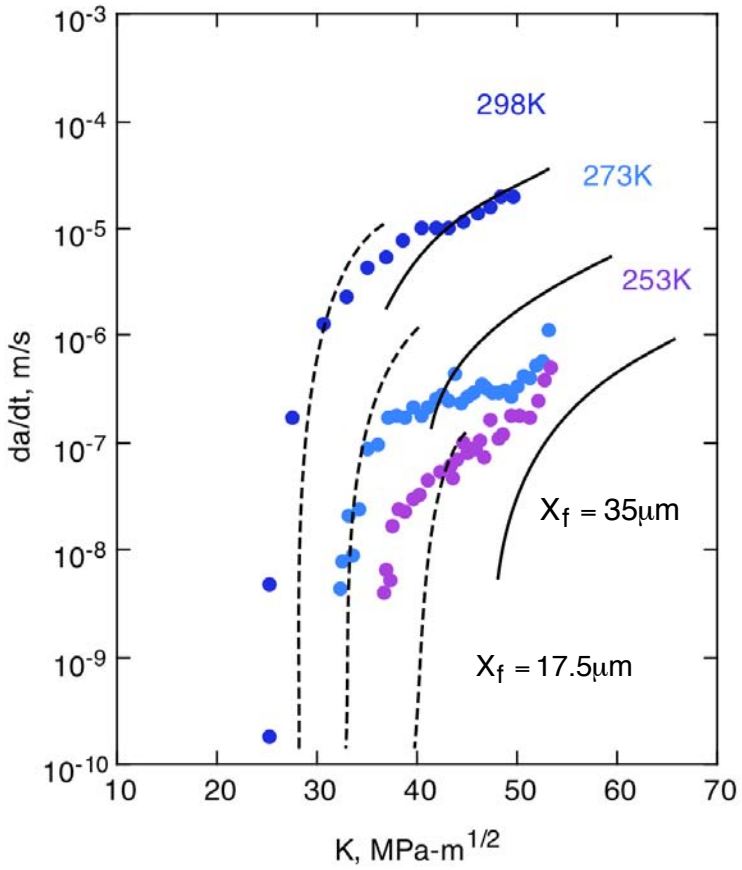

Temperature

The apparent activation energy for stage IIa crack growth at low temperatures correlates to diffusion through the IN903 lattice with trapping at gamma' precipitates.

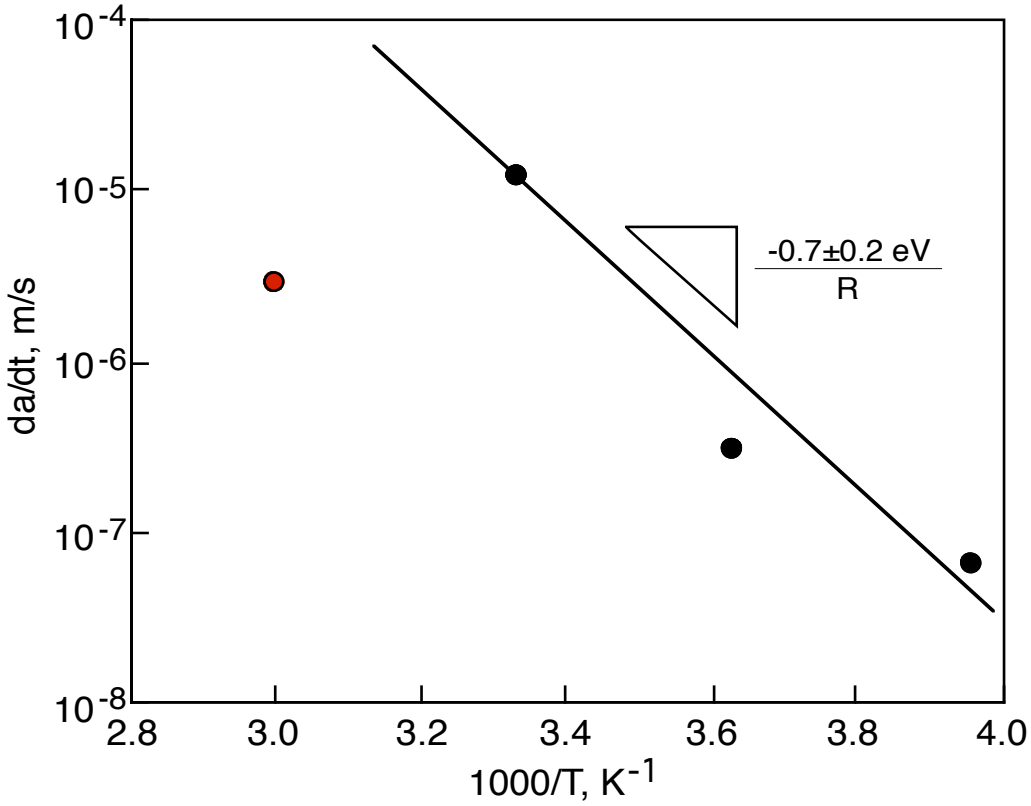

To a first approximation:

$$D_{eff} \approx D_o \exp\left[-\left(E_d + E_b\right)/RT\right]$$

E_d(IN903 matrix)= 0.5 eV

E_b(γ' trap binding energy)= 0.2 eV

Stage IIa slip band fracture in hydrogen charged samples is controlled by the diffusion of hydrogen.

Model provides a good fit to crack growth data in charged samples when fracture occurs by slip band failure.

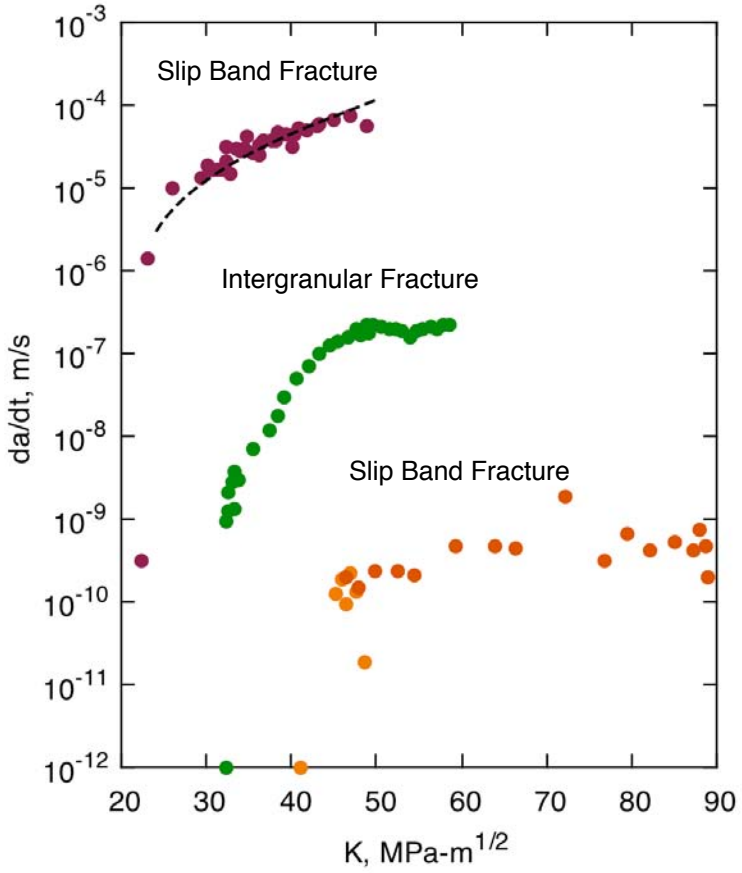

$D = 4.2e-15 m^2/s$

$\sigma_{shear} = 0.57UTS$

$X_f = 0.75\mu m$

$X_d = 75b$

$E_b = 0.2eV$

$\varepsilon_H = 0.16$

Predicted crack growth rates are in good agreement with measured values at room temperature.

Slip band fracture crack growth in hydrogen gas occurs at much lower rates than from redistribution of internal hydrogen.

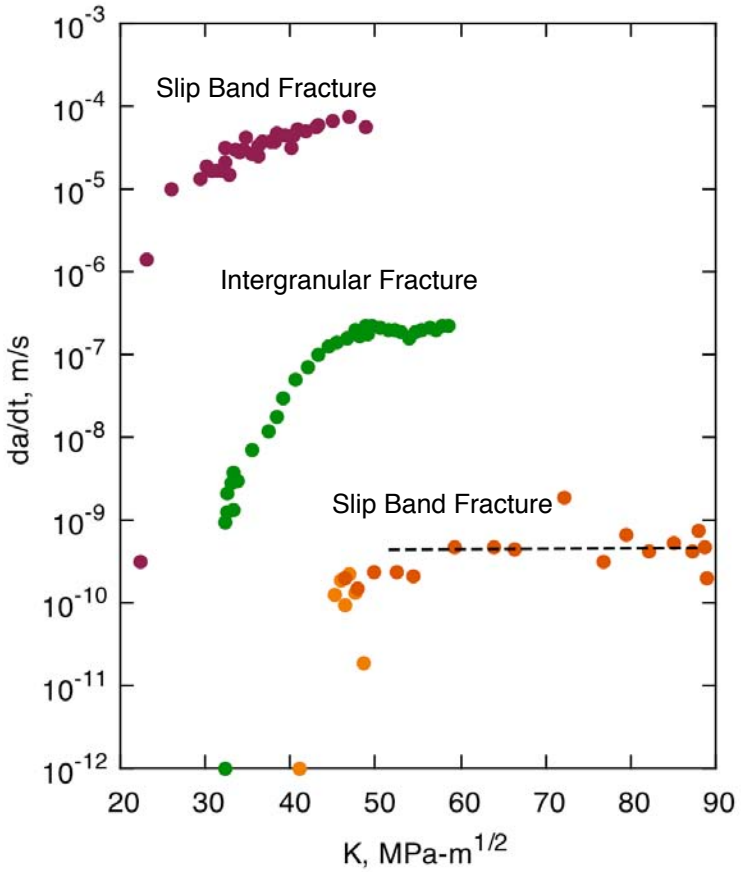

Fracture nucleates at cracked matrix carbides but proceeds rapidly back to the main crack

The crack tip concentration under these conditions is given by,

$$C_{cr} = C_o \exp\left(E_b / RT\right)\left\{1 - \mathrm{erf}\frac{X_d}{2\sqrt{Dt}}\right\}\exp\left(\sigma_h V_H / RT\right)$$

with erf(z)~z and $da/dt = X_f/t$

$$\frac{da}{dt} = \frac{4DX_f}{X_d^2}\left\{1 - C_r \Big/ \left[C_o \exp\left(E_b / RT\right)\exp\left(\sigma_h V_H / RT\right)\right]\right\}^2$$

$$D = 4.2e-15 m^2/s$$
$$X_f = X_d = 35\mu m$$
$$E_b = 0.2eV$$
$$\sigma_h = 2300MPa$$
$$V_H = 2cm^3/mol$$

The agreement between experimental values and model predictions indicates that matrix diffusion controls stage II crack growth in hydrogen gas.

Intergranular fracture initiates by decohesion/void formation at grain boundary carbides.

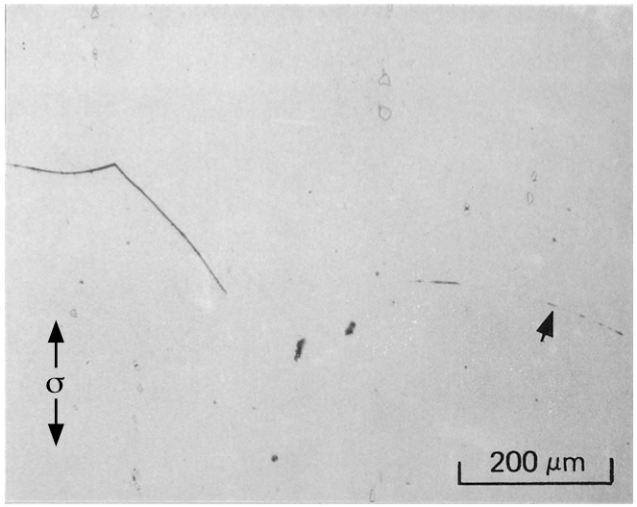

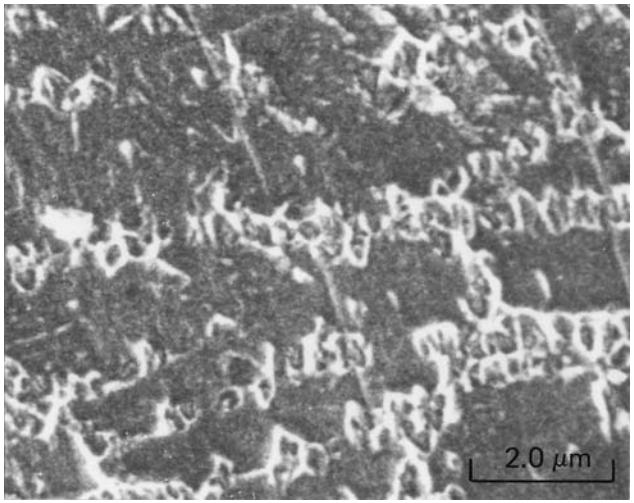

Tensile fracture cross sections show that intergranular fracture is stress controlled.

Crack growth at high hydrogen pressures occurs at much higher rates than at low pressures with a change in fracture from along slip bands to grain boundaries.

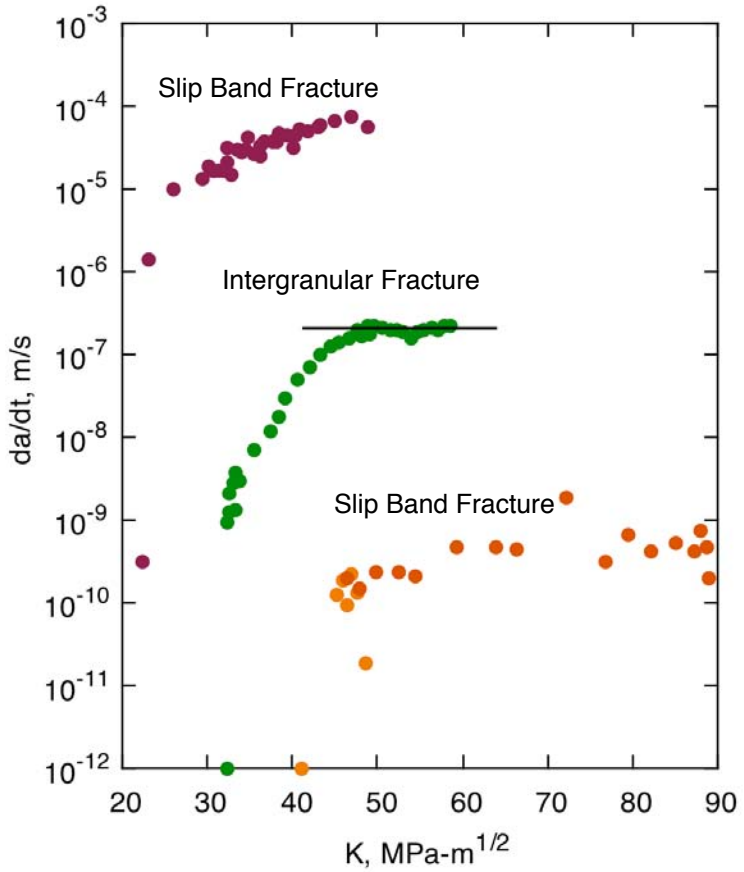

We can calculate an effective hydrogen diffusivity from measured crack growth rates

The expression for effective diffusivity under these conditions is,

$$D_{eff} = \left(\frac{da}{dt}\right)\frac{X_d^2}{4X_f\left\{1 - C_r / \left[C_o \exp(E_b / RT)\exp(\sigma_h V_H / RT)\right]\right\}^2}$$

with

$da/dt = 2x10^{-7}\,m/s$

$Xd = 2 \bullet X_f = 56\mu m$

$E_b = 0.2eV$

$\sigma_h = 2300MPa$

$V_H = 2cm^3/mol$

gives

$D_{eff} = 4.6x10^{-12}\,m^2/s$

The effective diffusivity is three orders of magnitude greater than the matrix diffusivity, suggesting that grain boundary diffusion controls crack growth.

Crack growth rates exhibit vastly different behaviors with respect to hydrogen concentration and hydrogen source.

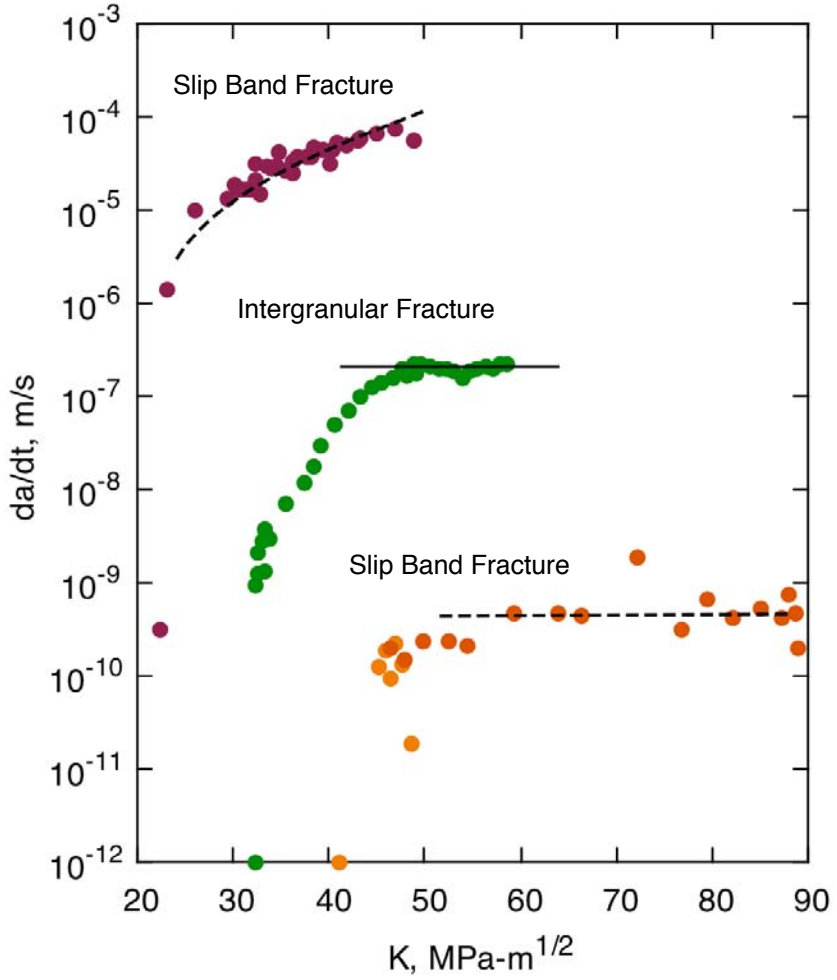

Slow Crack Growth Charged Samples
Slip Band Fracture

$D = 4.2e-15 m^2/s$
$X_f = 0.75 \mu m$
$X_d = 75b$
$da/dt \sim 10e-5 m^2 s$

Slow Crack Growth Hydrogen Gas
Intergranular Fracture

$da/dt = 2x10^{-7} m/s$
$X_f = 28 \mu m$
$Xd = 56 \mu m$
$D = 4.6e-12 m^2/s$

Slow Crack Growth Hydrogen Gas
Slip Band Fracture

$D = 4.2e-15 m^2/s$
$X_f = 35 \mu m$
$X_d = 35 \mu m$
$da/dt = 4.8e-10 m/s$

Microstructure, hydrogen source, and mode of transport interact to establish fracture processes and crack growth susceptibility.

Summary

Hydrogen reduces toughness and threshold values while fracture modes progress from microvoid coalescence to slip band failure and intergranular failure with increasing hydrogen concentration.

When normalized on crack tip concentrations and controlling fracture distance thresholds and toughness decrease monotonically with hydrogen concentration.

Crack growth rates exhibit markedly different behaviors with respect to hydrogen concentration and hydrogen environment.

- matrix diffusion controls crack growth in precharged samples
- matrix diffusion crack growth at low pressures in hydrogen gas
- grain boundary diffusion controls crack growth at high pressures in hydrogen gas.

Microstructure, hydrogen source, and mode of transport interact to establish fracture processes and crack growth susceptibility.

Acknowledgments

The support of Sandia National Laboratories is gratefully acknowledged.

Sandia is a multiprogram laboratory operated by Sandia Corporation, a Lockheed Martin Company for the United States Department of Energy's National Nuclear Security Administration under contract DE-AC04-94AL85000

The hydrostatic stress is determined from the maximum tensile stress at the characteristic distance for fracture at threshold.

$$\sigma_h = (2\sigma_{11} - \sigma_{ys})(1 + \nu) / 3$$

with σ_{11} defined by

$$\sigma_{11} = \sigma_{ys} [\, 0.3 / (X+0.1) \,][\, 0.04 / X \,]^{n/(n+1)}$$

where

$$X = l \; / (K_{TH} / \sigma_{ys})^2$$

with $l = 17.5\ \mu m$, $\sigma_{ys} = 1080$ MPa, and $n = 0.075$

$$V_H \approx 2.2 \text{ cc/mole}$$